ASTRONOMY & ASTROPHYSICS
SUPPLEMENT SERIES

Astron. Astrophys. Suppl. Ser. **143**, 227-263 (2000)

Comparison of 87 GHz solar polar structures with EUV and soft X-ray emission

S. Pohjolainen[1,2], **F. Portier-Fozzani**[3], **and D. Ragaigne**[4]

[1] DASOP, Observatoire de Paris, Meudon, France
[2] Metsähovi Radio Observatory, Helsinki Univ. of Technology, Espoo, Finland
[3] Equipe SOHO/EIT, Laboratoire d'Astronomie Spatiale, LAS-CNRS, Marseille, France
[4] DEA, Observatoire de Paris, Meudon, France

Received April 21, 1999; accepted January 21, 2000

Abstract. Polar radio brightenings at 87 GHz (3.5 mm) are compared for the first time with features seen in EUV and soft X-rays. The data consist of nearly simultaneous full disk images and maps from Metsähovi Radio Observatory, SOHO/EIT, and Yohkoh/SXT on 9 selected days near the solar minimum (1996-1997).

The observed radio brightenings corresponded to various features seen in EUV, such as diffuse or localized intensity enhancements (e.g., bright points and bases of polar plumes), and intensity depressions of varying sizes (e.g., coronal holes). Some of these features were also visible in soft X-rays. The visibility of radio bright coronal holes seemed to depend on how much of the polar area was exposed, due to the variation of the B_0-angle.

The observed radio depressions near the solar poles were very well correlated with coronal holes and other EUV and/or soft X-ray intensity drops. More than half of the coronal holes, or coronal hole-like intensity drops in EUV and soft X-rays, had radio brightenings inside them. Therefore coronal holes do not have uniform radio brightness at 87 GHz.

Many of the bright points seen at lower latitudes in the EIT and SXT images had no, or just faint, counterparts in the millimeter radio maps. It appears that for an EUV bright point to show up at 87 GHz it has to be bright and/or spatially large also in soft X-rays.

Key words: Sun: chromosphere — Sun: transition region — Sun: corona — Sun: radio radiation — Sun: UV radiation — Sun: X-rays

Send offprint requests to: S. Pohjolainen,
e-mail: pohjola@mesopy.obspm.fr

1. Introduction

Polar-cap brightenings in solar radio maps were first discovered in the 1970's (Babin et al. 1976; Efanov et al. 1980a, 1980b). Subsequently several studies were done using cm- and mm-wavelength data from, e.g., the Nobeyama 45-m telescope, the Nobeyama Radioheliograph, and the Metsähovi 14-m telescope. It has been claimed that the brightenings are restricted to a certain wavelength range, from 15 to 48 GHz (Gary et al. 1997), but the upper limit may simply be due to the lack of good quality observations at higher frequencies. Below 15 GHz the solar poles have been observed to appear darker, but at frequencies higher than 48 GHz both uniform brightness and local depressions have been observed (Gary et al. 1997; Kosugi et al. 1986), as well as the above mentioned brightenings (later paper by Moiseev & Nesterov 1987).

The studies of polar brightenings and depressions have included a variety of observed features, ranging from high-latitude polar-cap brightenings to any features observed above about 40 deg latitude. Also the appearance of coronal holes is very important in polar regions. Along with the question whether polar brightenings do appear at high frequencies (shorter than 6 mm), a puzzle exists on the origin of the brightenings: are they associated with limb brightening (Shibasaki 1997), coronal holes (Brajša et al. 1996), faculae (Riehokainen et al. 1998), magnetic features (Kosugi et al. 1986; Gopalswamy et al. 1999), atmospheric structures (Hiei 1987), polar plumes (Gopalswamy et al. 1992), or something else?

The starting point of this study was the fact that for the first time at 87 GHz (3.5 mm), the solar radio maps observed with the upgraded Metsähovi Radio Observatory 14-m telescope showed polar brightenings and depressions. We present here an analysis of data from 9 separate days

observed near the solar minimum (1996-1997), with good imaging capabilities at 87 GHz.

2. Observations

2.1. Metsähovi observations

The Metsähovi radio telescope was upgraded in 1992-1994, and at present the surface accuracy is 0.1 mm (rms). The 14-meter antenna gives 1.0 arcmin spatial resolution (i.e. HPBW beam size) at 87 GHz (3.5 mm). The maps are made by scanning the Sun in right ascension, by changing declination between the scans. The full solar disk is scanned in 9 minutes in the "fast map" mode, which makes 29 scans, 91 samples each. The flux resolution for this study was estimated from nearby active region track files. Track files are made by pointing the beam to a selected region on the solar disk and by measuring the flux density (sampling rate 20 samples/s). By using active region track files we get a maximum amount of noise fluctuations, as fluctuations from the active region itself are included. Large noise levels can therefore be the result of very active regions on the disk. A large noise level can affect the quality of the map (i.e., the dynamic range). An example of a low-quality radio map is in Fig. 8, from May 20, 1997. The variation in this case is most probably instrumental, and depends on the set-up. Set-ups may be changed between the days or between the observing runs. In the analysed radio maps the flux resolution varied from 0.3% to 0.5% of the quiet Sun flux, depending on the observing run in question.

No absolute flux calibration is done during the Metsähovi solar observations, but the quiet Sun brightness temperature has previously been estimated to be around 7200 K at 87 GHz (see Pohjolainen & Urpo, 1997), giving a brightness temperature resolution of $22 - 36$ K for this study. The observed flux density, which is directly related to brightness temperature, is expressed in the tables as a percentage of the quiet Sun level, which is determined from the A/D converter counts. For example, on April 12, 1996 the quiet Sun level was estimated to be at 7240.0 A/D count units, which is equivalent to the estimated 7200 K brightness temperature. A bright area showing a 1.009 relative intensity is therefore 0.9% above the quiet Sun level, i.e., is showing a brightness enhancement of 64.8 K.

The solar maps that are presented here are the "raw" maps, without any deconvolution methods applied. Because the beam is not sharp but more like a broad Gaussian with wings (sidelobes), an artificial limb darkening and an artificial sky brightening are observed near the true edge of the solar disk (see Lindsey & Roellig 1991). The effect can be seen as the dark ring in the 87 GHz radio maps inside the circle which marks the optical solar limb, and as additional emission outside the solar limb. We analyse here only those brightenings and depressions that were well outside this effect (i.e. well inside the solar disk). The artificial limb darkening makes it impossible to see the features as high as the polar caps, but because of the changing B_0 angle, features up to 70 deg in latitude (at 0 longitude) can be discerned.

Table 1. EIT bandpasses for the observations

Wavelength	Ion	Temperature
304 Å	He II	8.0 10^4 K
171 Å	Fe IX, X	1.3 10^6 K
195 Å	Fe XII	1.6 10^6 K
284 Å	Fe XV	2.0 10^6 K

2.2. SOHO-EIT observations

The Extreme Ultraviolet Imaging Telescope (EIT) onboard the *SOHO* spacecraft, images the corona in four EUV wavelengths (Delaboudiniere et al. 1996). From EUV lines – which represent different ion transitions – the chromosphere (He II), the transition region (Fe IX/X) and the corona (Fe XII, Fe XV) are imaged, see Table 1. Temperature diagnostics are made by wavelength ratios (Neumark et al. 1997), and 3-D coronal structure evolution is studied by comparing filter images (Portier-Fozzani et al. 1996).

The selected four EIT images per day – observed as close as possible to the radio observations – were taken with filter Clear or Al+1. The EIT pixel resolution is 2.6 arcsec. The full Sun images were either 1024×1024 (full resolution, denoted "F" in Table 2) or 512×512 (half resolution, denoted "H" in Table 2).

The EIT images were calibrated using the usual software methods described in Moses et al. (1997). To remove the shadow of the tiny grid that supports an aluminium filter standing in front of the CCD camera, included in all EIT images, smooth filtering using a local median filter was preferred (Portier-Fozzani et al. 1996). More details concerning the EIT calibration and in flight use can be found in Moses et al. (1997), Newmark et al. (1997), Defise (1999), and Portier-Fozzani (1999).

2.3. Yohkoh SXT observations

The Soft X-ray Telescope (SXT) onboard the Yohkoh satellite observes the solar corona through several different filters (Tsuneta et al. 1991). The broad-band instrument is sensitive over a range of energies between 0.25 and 4 keV. The corresponding coronal temperatures are in the range of $2 - 20$ MK. In the case of the quiet solar corona, the temperatures are at the lower end of this scale.

We used SXT full frame images, taken with the AlMg and Al.1 filters near the times of the radio observations,

with the longest available exposure times, in order to get the faint features visible. The full frame SXT images were observed either in Half resolution (denoted "H" in Table 2) with 4.9 arcsec pixel size, or in Quarter resolution (denoted "Q" in Table 2) with 9.8 arcsec pixel size. The exposure times varied between 0.6 s (August 13, 1996) and 30.2 s (April 12, 1996). The SXT images were corrected for dark noise and particle hits.

2.4. Other wavelength data

As it is well known than H_α dark filaments can cause radio depressions (Vršnak et al. 1992), we checked from the H_α images in the Web (http://sohodb.nascom.nasa.gov/cgi-bin/synop_query_form) that no filaments were present where we had radio depressions. Therefore the radio depressions analysed in this study must be caused by some other mechanism than an overlaying absorbing dark filament.

Coronal holes and their borders are sometimes difficult to define. We used also other wavelength data from the Web, when available, to check the locations under study. Especially He I (10830 Å) images were useful for this purpose.

2.5. Selection of data and error analysis

We went through the radio maps measured at Metsähovi at 87 GHz (3.5 mm) in 1996 and 1997, and selected the ones that had close-in-time observations at least with one of the EUV wavelengths, observed by the EIT. In this way 9 radio maps from 9 days were selected, see Table 2. A lot more radio maps are available if nearness in time is not a requirement.

All four EIT wavelengths were then analysed, to confirm the structural classification in EUV. In the analysis the maximum time difference between a radio and an EUV map was 1.5 hours, but in that case more close-in-time observations were available at the other three EUV wavelengths, and we checked that the observed features were consistent. SXT maps were selected on the basis of being taken as near as possible to the selected radio and EUV maps, and with the longest available exposure times.

The tops and the bottoms of the selected radio brightenings and depressions, respectively, were given heliographic coordinates. The positions (latitude, longitude) and intensities (relative to the quiet Sun level) for altogether 104 radio sources are given in Tables 3–11, for each of the days separately. In the tables, EIT and SXT structures are defined for the radio locations and their surrounding area.

In comparing the features in radio and in EUV one should be aware of the fact that the spatial resolution at 87 GHz is rather poor, about 1 arcmin (HPBW). Radio emission sources that are located within the 1 arcmin beam area will be convolved, and this means that the true peak brightness can be "off" the given coordinates. The scanning technique poses problems as well: pointing errors are common when using heavy antennas at high speed. To overcome the "off" pointing, all features within the 1 arcmin beam were classified and listed.

The Metsähovi scan map method was originally developed for 37 GHz, with a much larger beam size. At 87 GHz the beam size is smaller than the separation between scans, 1.2 arcmin. This can mean missing some flux, if a very small point source is located just in between the scan paths. However, the non-symmetrical main beam and strong sidelobes usually reduce this problem. Atmospheric changes between separate scans can also cause defects, which are usually seen as the sawed edge of the solar limb.

Another, a much larger error, comes from the determination of the center of the radio Sun. Due to the non-symmetrical beam and errors in scanning, the radio Sun is not a perfect circle, and the person making the data reduction is very much responsible for putting the center point to the "right" position. Our data set was analysed separately by two different people, and the maximum difference in coordinate determination was 10 degrees in heliographic longitude, which was caused by moving the center point in an East-West direction. However, this kind of difference in coordinates was extremely rare.

Also, a small bright point in a cool dense region will be diluted in a large radio beam, and will not necessarily show up. If sources looking similar in EUV are not both detected in radio, one must look for differences in temperature and/or density. The basics of radio emission and antenna beams can be found in, e.g., Dulk (1985) and Pohjolainen (1996). To explore the effects of the different resolutions of the two instruments, a test was made by plotting EIT images degraded into radio resolution. It was found that structural mixing was present in some cases, but also good fit to the radio images was found (Pohjolainen et al. 1999a).

3. Analysis and results

Nine solar radio maps, from 9 different days, observed in 1996–1997 were analysed for this study. The coordinates and fluxes of radio bright and depressed (relative to the quiet Sun level) areas near the polar zones were listed, as described in Sect. 2.5. Also some strong active regions at lower latitudes were given coordinates, mainly to check the accuracy of the radio coordinate determination.

The listed radio source locations were analysed in all EUV wavelengths, and all EUV features seen within the 1 arcmin radio beam were listed. The identification of EUV features was mainly based on coronal images (171/195/284 Å). The Fe IX/X line (171 Å) was usually checked first, and then compared with images at other

Table 2. Selected radio, EIT, and SXT maps for comparing polar structures

Date	87 GHz radio map UT	EIT map UT				SXT map UT	
		He II	Fe IX/X	Fe XII	Fe XV	AlMg	Al.1
Apr. 12, 1996	13 : 57 − 14 : 05	14:50(F)	14:28(F)	15:12(F)	14:06(F)	13:52(H), 14:23(Q)	13:55(H)
Apr. 15, 1996	12 : 05 − 12 : 13	13:12(F)	12:14(F)	12:20(F)	13:01(F)	11:18(H), 13:13(H)	
Aug. 09, 1996	07 : 23 − 07 : 32	07:40(H)	07:24(H)	07:34(H)	07:30(H)	07:00(H)	06:48(H)
Aug. 13, 1996	12 : 31 − 12 : 39	12:35(H)	12:30(H)	12:34(H)	12:32(H)	12:39(Q), 12:48(Q)	
Aug. 14, 1996	12 : 55 − 13 : 03	12:35(H)	12:30(H)	12:34(H)	12:32(H)	12:53(H)	12:39(H)
May 20, 1997	13 : 03 − 13 : 12	13:18(F)	13:00(F)	13:12(F)	13:06(F)	12:53(Q), 13:15(Q)	
Aug. 08, 1997	11 : 30 − 11 : 39	13:28(F)	13:10(F)	11:47(F)	13:16(F)	11:04(Q), 12:17(Q)	
Aug. 27, 1997	12 : 13 − 12 : 22	13:19(F)	13:01(F)	12:15(H)	13:07(F)	12:10(H), 12:55(H)	12:53(H), 13:08(H)
Aug. 28, 1997	07 : 16 − 07 : 24	07:18(F)	07:00(F)	07:12(F)	07:06(F)	07:06(H), 07:23(H)	07:04(H), 07:21(H)

wavelengths. The same procedure and listing was done with the soft X-ray images.

The classification of EUV and soft X-ray features was based on intensity, spatial scale, and general "lookout". We determined the quiet Sun level in each of the images, and the enhanced/reduced brightness was determined relative to this. One effect of this method was that very few of the analysed locations were determined to be "quiet Sun", as it was defined to be practically one intensity value. Also, as the radio beam area consists of 30 − 400 SXT or EIT pixels (depending on the observing mode), we did not try to give any "average" intensity value for the EUV/soft X-ray features.

With this method each radio location could have more than one possible counterpart in EUV and soft X-rays (indicated by "/" in Tables 3–11). The problem of multiple sources within the radio beam is clearly seen in the polar region EUV blow-up image, in Fig. 1. Tracking problems with radio antennas can sometimes cause displacements in the beam position, and therefore we also looked for strong emission sources nearby the assumed antenna beam position. The "nearby" features are also listed in Tables 3–11. The radio maps are presented in Figs. 2, 5, ... 26, the soft X-ray images in Figs. 3, 6, ... 27, and the EIT images in Figs. 4, 7, ... 28.

The quiet Sun radio emission at 87 GHz (3.5 mm) originates from chromospheric heights, and has an estimated brightness temperature of 7200 K. The emission is mostly due to thermal bremsstrahlung. However, radio emission can also be produced at greater heights if the plasma density and temperature are high enough in, e.g., coronal loops. Besides thermal emission, other emission mechanisms may also be present. There has been some discussion on possible synchrotron sources and plasma emission connected with coronal holes (e.g. Shevgaonkar et al. 1988).

In EUV coronal lines, the intensity is proportional to the emission measure, which is related to the temperature and the density. The iron lines are optically thin. With the iron lines different temperatures of the corona can be observed. The image appears darker where the temperature is lower (e.g., filament channels) or the density is smaller (e.g., coronal holes, where the plasma can escape along the open magnetic field lines). Fe XII is adapted to observe the "usual" corona, while Fe XV observes the more hot temperatures. Structures in Fe IX/X always appear with narrow shapes (such as loops). This transition region line is very important for the analysis, as it shows the evolution of the topology and the morphology at intermediate temperatures between the photosphere and the corona. The He II line at 304 Å is an optically thick line. This chromospheric line is mixed with a coronal Si IX line.

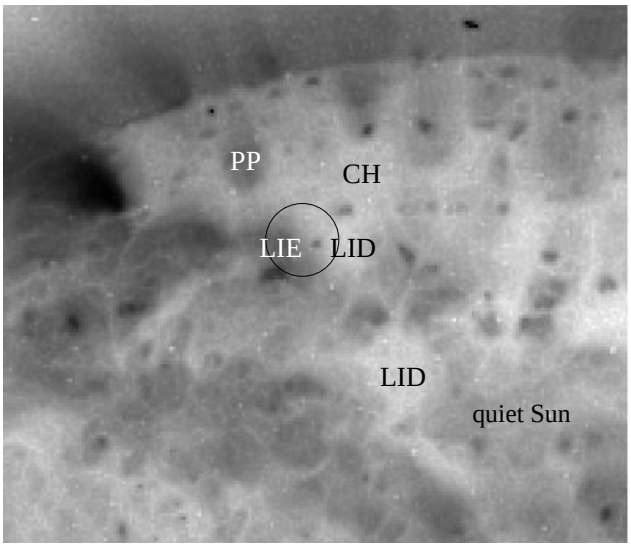

Fig. 1. Polar region on August 27, 1997, at 13:01:03 UT in Fe IX/X line (reversed colours). The cicle has 1 arcmin radius and shows the size of the radio beam. Depending on the location, there is a possibility of having several EUV structures within the beam. This location was classified as a local intensity enhancement (LIE, in dark colour), although it is nearby a local intensity decrease area (LID, in white colour). The contrast in the image has been enhanced, to show more clearly all the tiny EUV structures

The Yohkoh/SXT was mainly designed for observing flares and other transient phenomena. The quiet Sun

emission, with changing features but low count rates, is therefore more difficult to analyse. Some studies of polar coronal holes have been made with the SXT (see, e.g., Foley et al. 1997), but these have required longer than normal-mode exposure times and summing up of images over long periods. Coronal hole temperatures in soft X-rays have been found to be similar to the values for the nearby quiet corona, but with electron density values about 3 times lower (Hara et al. 1994). We did not do any temperature or emission measure analysis because of the long image intervals and low count rates in some of the individual images.

One should also note that no comparison of features was done between the EIT and the SXT images. We compared only radio and EUV, and radio and soft X-ray emission sources in the given solar coordinates, but within the radio beam. Since the radio resolution is so different from the two others, comparison of a single location in high resolution images might give different results.

Quiet Sun structures are usually considered to be very stable, and not change much in time. Polar plumes may stay the same for hours, and radio depressions and brightenings have been used for, e.g., determining the solar rotation rate at high latitudes. However, when comparing the radio and soft X-ray images we found that the borders of coronal holes can change their position within some tens of minutes. On April 12, 1996, at 13:52 UT the radio brightening 3S was situated in the coronal hole border area, near a soft X-ray brightening, but in the later SXT image at 14:23 UT the radio position had moved inside the coronal hole area. On August 9, 1996, the radio bright position 4N moved from coronal hole border area to a diffuse bright area within 12 minutes, and on August 8, 1997, positions 1N and 6N moved from the coronal hole border area to inside the coronal hole, within about an hour. Therefore one should be very careful in comparing coronal hole border areas when the time differences between images are larger than the order of tens of minutes.

3.1. Radio – EUV

The radio locations included 81 brightness peaks and 23 depression centers. For half of the radio locations (51/104) it was possible to determine a sole counterpart from the EIT images. For the rest of the cases two or possibly more different features were present within the estimated radio beam. We would have to know the temperatures and densities of each of these features to be able to determine how much they contributed to the radio emission.

The EUV regions listed in Tables 3–11 were classified as:

- AR = Active Region,
- BP = Bright Point,
- PP = Polar Plume (or a group of plumes),
- LIE = Localized Intensity Enhancement,
- LID = Localized Intensity Decrease,
- CH = Coronal Hole.

Active regions (AR) were classified with the help of NOAA active region listings from the Solar Geophysical Data. Also large EUV and radio bright regions with complex loop structure were classified as ARs, even if they were not listed by NOAA. These regions were much larger than bright points and much more intense than localized intensity enhancements (see below). The tops of the hot loops in ARs usually show thermal radio emission. During long duration events and flares, also footpoint brightening is observed at cm wavelengths (Hanaoka 1994).

Bright points (BP) are bright individual features sometimes seen in coronal holes. Bright points can also be seen over diffuse bright structures, all over the solar disk. The sizes of BPs are usually $10 - 50''$. Simultaneous EUV and soft X-ray observations have shown that the regions of peak emission are not always cospatial, suggesting a complex structure of small-scale loops, at different temperatures (Habbal et al. 1990). EUV and soft X-ray bright points have been found to be associated with magnetic bipolar regions, but cm-radio observations have shown some association between radio bright points and unipolar magnetic structures (Kundu et al. 1988). EUV bright points have not been studied much at radio wavelengths.

Polar plumes (PP) are bright individual features seen in polar coronal holes (DeForest et al. 1997), and sometimes in coronal holes that extend to equatorial heights (Allen et al. 1997). They can also appear in groups. The 3-D structures of polar plumes are very well seen with EIT. Polar plumes have not been detected previously at millimetric radio wavelengths. A study by Nindos et al. (1999) discovered centimeter radio emission arising between the plumes in polar regions.

Localized intensity enhancements (LIE) are brighter than the quiet Sun and less bright than ARs. They are also larger than BPs. They exist outside coronal holes and active regions, and include sometimes diffuse areas like the borders of coronal holes. Magnetograms for these areas give no definite polarities. The brighter features could be loop structures that are not seen due to the EIT spatial resolution. Temperatures given by EIT for these structures are between $1 - 1.6$ MK.

Localized intensity decreases (LID) are small – a few arcmin diameter – regions that are less bright than the quiet Sun. These small "holes" can be found all over the solar surface. The existence of small coronal holes has been suggested previously by Bohlin (1976).

Coronal holes (CH) are seen as dark regions in EUV and soft X-rays, and as bright regions in the He I absorption line. The density and/or temperature is usually lower than in the surrounding corona. There has been some debate on whether CHs can be identified as open field line areas (Obridko & Shelting 1999), but at least for statistical purposes this definition can be used. Coronal holes are usually seen as depressions at centimeter

wavelengths, but several studies have shown radio bright coronal holes (Gopalswamy et al. 1999; Brajša et al. 1996).

The radio brightness enhancements (81) correlated with the following EUV features: active regions (3), polar plumes (3), localized intensity enhancements (17), localized intensity decreases (12), coronal holes (9), and mixtures of features (37).

The radio depressions (23) correlated with the following EUV features: localized intensity enhancements(2), localized intensity decreases (13), coronal holes (2), and mixtures of features (6).

3.2. Radio – soft X-rays

The structures seen in the Yohkoh SXT images were listed similarly, but to avoid confusion between the EUV and soft X-ray features we named some of the soft X-ray features differently. Brightness enhancements and less bright regions in soft X-rays are usually spatially larger (reflecting also the instrument resolution) than in EUV, and therefore we dropped the term "localized". The soft X-ray features were listed as follows:

- AR (as in EUV),
- BP (as in EUV),
- enhanced brightness (above the quiet Sun brightness),
- reduced brightness (below the quiet Sun brightness),
- CH (as in EUV).

The radio brightness enhancements (81) correlated with the following soft X-ray structures: active regions (4), bright points (8), enhanced brightness (39), reduced brightness (5), coronal holes (16), and a mixture of features (9).

And the radio depressions (23) correlated with the following soft X-ray structures: enhanced brightness (2), reduced brightness (9), coronal holes (8), quiet Sun (3), and a mixture of structures (1).

4. Summary of comparisons

We have observed polar brightenings at 87 GHz (3.5 mm wavelength), with a typical $0.5-1.5\%$ brightness enhancement over the quiet Sun. Taking an average quiet Sun brightness temperature of 7200 K at 87 GHz, we get brightness enhancements in the scale of $35-110$ K. In comparison, the active regions observed at $20-30$ degrees in latitude in the same solar maps showed $1-4\%$ brightness enhancements.

Radio brightenings were found to correlate with several different types of structures seen in EUV (see Sect. 3 for the exact numbers).

- Localized intensity enhancements (LIE – 17 locations): At 87 GHz, they often showed a brightness enhancement of about 1%. The borders of coronal holes often show diffuse emission, as the open field line areas change into a border of closed lines.
- Localized intensity decreases (LID – 12 locations): Surprisingly many of the radio enhancement peaks were located inside the small less bright regions. The corresponding radio brightenings varied in intensity, between 0.2% and 2.4%. However, these EUV reduced brightness areas usually had very small spatial size, and were often surrounded by diffuse matter or small bright areas that could contribute to the radio flux, so the connection can be ambiguous.
- Coronal holes (CH – 9 locations): In our study the radio brightenings for coronal holes were between 0.4% and 2.3%. Radio brightenings inside coronal holes were linked with the changes in B_0 angle: when more of the polar regions and coronal holes were visible, the clearer were the radio brightenings inside them. On April 12, 1996, on April 15, 1996 (see Figs. 29 and 30 for close-ups), and on May 20, 1997, radio bright regions were located inside the southern CHs, and on August 9, 1996, and on August 8, 27, and 28 the radio bright regions were detected in the northern CHs.
- Polar plumes (PP – 3 locations): The radio enhancements for the three locations that corresponded to plumes were 1.0% (location 3N on August 13, 1996), 1.4% (location 2N on August 13, 1996), and 1.5% (location 2N on August 14, 1996). The fact that plumes are inside coronal holes, which are cool and less dense, and that the plumes may not fill the whole radio beam area and may be diluted within the beam, make this radio signature even more significant.
- Active regions (AR – 3 locations): The tops of the loops in EUV were seen as radio brightenings, as expected. Active region loops showed higher brightness temperature in radio $(3.6-4.0\%)$ than, e.g., the plumes.
- Bright points (BP – no definite detections): Three radio bright polar locations could be correlated to EUV bright points, with the help of soft X-ray images (EUV-only analysis classified them as mixed features). These were location 2S on August 9, 1996 (2.1% enhancement), location 1N on August 13, 1996 (1.3% enhancement), and 1S on August 14, 1996 (2.1% enhancement). Yohkoh SXT also showed 4 bright points that were not classified as those in EUV, on April 12, 1996 (locations 3N with 0.6% and 4N with 0.4% radio enhancements), on August 9, 1996 (location 2S with 2.1% radio enhancement), and on May 20, 1997 (location 3S with 0.6% radio enhancement).

Radio depressions (23 altogether) at 87 GHz showed $0.5-2.0\%$ ($35-145$ K) brightness drops, and were clearly correlated with coronal holes, localized intensity decreases, coronal hole borders seen as intensity enhancements, or a combination of these three features in EUV. The soft X-ray images confirmed the correlation: of the 23 radio depressions 17 were located within coronal holes or reduced brightness regions. And further, if we look at the

classifications in both EUV and soft X-rays, only one location (7S, on August 13, 1996) was not connected to coronal holes. Therefore we can say that radio depressions in 3.5 mm are connected to the coronal hole phenomenon.

However, this is not so in the reverse situation: coronal holes and local less bright regions seen in EUV, and in soft X-rays, were often seen as brightenings at 87 GHz. This study showed 15 radio depressions vs. 22 radio brightenings for coronal hole-like EUV sources, and 17 radio depressions vs. 21 radio brightenings for coronal hole-like soft X-ray sources.

X-ray bright points have previously been detected at cm-wavelengths, using observations made with the Nobeyama Radioheliograph and the VLA (Nitta et al. 1992; Kundu et al. 1994). We now report detection of bright points also at 3.5 mm wavelength. A few radio brightenings correlated with bright points that were strong both in EUV and soft X-rays. Besides the 3 that were reported earlier, there were some found at lower latitudes: location S22W06 on August 9, 1996, and location N35E33 on August 13, 1996.

However, many of the bright points seen on the solar disk in the EIT and SXT images had no, or just very faint, counterparts in millimeter waves. By looking at some low latitude bright points we were able to conclude that even if the bright points were strong in EUV, they would not show up in millimeter radio if they were not strong enough (N56E30 on August 9, 1996), or spatially large enough (S42W26 and S57E24 on April 15, 1996 – see Figs. 29 and 30), in soft X-rays.

Also, if the bright points lie inside coronal holes instead of bright diffuse sources, their radio flux will be diminished (N16W17 and S30E33 on April 12, 1996). There were also cases where no obvious reason could be found for why some bright points showed up in radio (S27W13 and S30W30 on August 28, 1997) and some did not (S15W13 on the same day), see Fig. 31.

5. Discussion

Quiet Sun radio emission at 87 GHz originates from the upper chromosphere, as free-free emission from a plasma at a temperature of about 7200 K. Thermal radio emission corresponds to the density and temperature of plasma, and the source height for radio emission can only be determined if the source is located over the limb. Also, radio brightening can be suppressed by cool dense material high in the corona, as is the case for the locations of H_α dark filaments.

In our study a large number of coronal holes appeared as brightness enhancements in radio. However, many coronal holes appeared also radio depressed. Therefore coronal holes in general cannot be defined as radio bright at 87 GHz. Many of the localized intensity decreases (LIDs) seen in EUV also appeared radio bright – but not all of them. In many cases structural mixing was present, i.e., more than one EUV feature appeared within the radio beam. In some of the EIT maps it was possible to see a patchwork of small "holes", and the radio enhancement peaks were located inside them. The observed diffuse bright soft X-ray emission over the EUV LIDs could be explained by hot coronal material, or by time differences in the observations, or by projection effects that could change the soft X-ray source positions.

Thermal radio emission is enhanced with growing density and/or temperature, and can be formed at any height in the solar atmosphere above the critical plasma density level. Therefore local dense and relatively hot (but cooler than needed for EUV lines), or less dense and very hot (possible to see in soft X-rays) regions would show out as radio brightenings. In our data a few locations were seen as dark coronal holes in the hot Fe lines, but when viewed in the chromospheric He II line, small local brightenings were found. Some of the coronal hole radio brightenings could therefore be formed at temperatures below the He II line.

In a recent paper Gopalswamy et al. (1999) suggest that coronal holes are seen as radio brightenings only if there are flux concentrations present in unipolar magnetic regions. The authors connect microwave enhancements with a combination of a smooth component, which probably comes from network cell interiors, and other more compact sources. Unfortunately the spatial resolution is too poor in our case to be able to separate the possible different components. The magnetograms for our data set are to be analysed, to see if there is a difference between the radio enhancements and depressions for coronal hole-like areas.

A study by Nindos et al. (1999), comparing 17 GHz radio brightenings with EIT features, did not find a one-to-one correlation between compact radio sources and bright EUV features either. They also suggested an association between the He II and diffuse polar cm-wave emission, which would mean that the radio emission comes from heights below the 80000 K layer, and not from the corona. The suggestion that in some cases the cm- and mm-wave radio emission has its origin at relatively low heights in the solar atmosphere has also been supported by the recent finding that 87 GHz radio bright regions are often associated with EUV, and even UV bright points, observed with the 0.5 arcsec pixel resolution of the TRACE satellite (Pohjolainen et al. 1999b).

Our data set showed that bright points, and sometimes even plumes, can be detected at 3.5 mm wavelength. However, many of the plumes were too high in latitude to be visible in the radio maps (limit of about 70 degrees). The bright points that did show up well in the mm-radio maps were intense both in EUV and soft X-rays. Also some indication of emission below 80 000 K was detected inside the coronal holes.

It has been suggested that cm-wave radio brightenings near the solar poles and inside coronal holes – as they are most probably connected to temperature enhancements in the chromosphere – may be related to the origin of solar wind. Millimeter wave emission has its origin even deeper down in the chromosphere, and our finding of mm-wave coronal hole brightenings may be a further proof of heating processes taking place in the chromosphere, that are necessary for solar wind plasma flows.

Due to the low spatial resolution of the available mm-wave radio observations it is difficult to determine any single feature to be the cause for radio brightenings. Our study suggests that bright points and polar plumes, as well as unresolved EUV and soft X-ray brightenings could be associated with radio brightenings. We also discovered radio bright regions inside coronal holes, with no obvious features causing them. This suggests that a closer look with good spatial resolution will be needed in the whole spectral range – from UV to soft X-rays – combined with magnetograms, to discover the physical counterparts for the brightenings.

Acknowledgements. We thank the anonymous referee for his constructive suggestions and helpful comments that improved the paper significantly. Part of this work was done at Metsähovi Radio Observatory, during D.R.'s training period. S.P. is supported by the Academy of Finland Contract No. 42576. F.P-F was supported in his work also by private foundations. SOHO/EIT was build by an international consortium involving ESA and NASA, under the supervision of J.P. Delaboudinière (PI). Yohkoh is a Japanese solar mission, with several internationally operated instruments. The SXT images were analysed using the Yohkoh Data Archive Centre (YDAC) at Mullard Space Science Laboratory. The alignment of multi-wavelength images for some of the figures was done with the help of Object-Based Methods for Analyzing Solar Images developed by D. Zarro.

References

Allen M.J., Oluseyi H.M., Walker A.B.C., Hoover R.B., Barbee T.W., 1997, Solar Phys. 174, 367
Babin A.N., Gopasyuk S.I., Efanov V.A., Kotov V.A., Moiseev I.G., Nesterov N.S., Tsap T.T., 1976, Izv. Krymsk. Astrofiz. Obs. 55, 3
Bohlin J.D., 1976, Natural History 85, 68-70
Brajša R., Pohjolainen S., Ruždjak V., Sakurai T., Urpo S., Vršnak B., Wöhl H., 1996, Solar Phys. 163, 79
Defise J.M., 1999, Ph.D. Thesis, Belgium
DeForest C.E., et al., 1997, Solar Phys. 175, 393
Delaboudinière J.-P., et al., 1996, Solar Phys. 162, 291
Dulk G., 1985, ARA&A 23, 169
Efanov V.A., Labrum N., Moiseev I.G., Nesterov N.S., Stewart R., 1980a, Izv. Krymsk. Astrofiz. Obs. 61, 52
Efanov V.A., Moiseev I.G., Nesterov N.S., Stewart R., 1980b, in Kundu M.R. and Gergely T.E. (eds.). Radio Physics of the Sun, IAU Symp. No. 86. Reidel, Dordrecht, p. 141
Foley C.R., Culhane J.L., Acton L.W., 1997, ApJ 491, 933
Gary D.E., Enome S., Shibasaki K., Gurman J.B., Shine R.A., 1997, BAAS 29, 8.01
Gopalswamy N., Schmahl E.J., Kundu M.R., 1992, Proc. First SOHO Workshop, Coronal Streamers, Coronal Loops, and Coronal and Solar Wind Composition, p. 113
Gopalswamy N., Shibasaki K., Thompson B.J., Gurman J., DeForest C., 1999, JGR 104, 9767
Habbal S.R., Dowdy J.Jr., Withbroe G.L., 1990, ApJ 352, 333
Hanaoka Y., 1994, Proc. of Kofu Symp., NRO Report 360, 181
Hara H., Tsuneta S., Acton L., et al., 1994, PASJ 46, 493
Hiei E., 1987, PASJ 39, 937
Kosugi T., Ishiguro M., Shibasaki K., 1986, PASJ 38, 1
Kundu M.R., Schmahl E.J., Fu Q.-J., 1988, ApJ 325, 905
Kundu M.R., Shibasaki K., Enome S., Nitta N., 1994, Proc. of Kofu Symposium, NRO Report No. 360, 79
Lindsey C.A., Roellig T.L., 1991, ApJ 375, 414
Moiseev I.G., Nesterov N.S., 1987, Izv. Krymsk. Astrofiz. Obs. 77, 83
Moses D., et al., 1997, Solar Phys. 175, 571
Neumark J., et al., 1997, Am. Astron. Soc. Meeting 191, 73.07
Nindos A., Kundu M.R., White S.M., Gary D.E., Shibasaki K., Dere K.P., 1999, AAS 194, 32.07
Nitta N., Bastian T.S., Aschwanden M.J., Harvey K., Strong K., 1992, PASJ 44, 167
Obridko V.N., Shelting B.D., 1999, Solar Phys. 187, 185
Pohjolainen S., 1996, Metsähovi Radio Res. Stat. Report Series A 24, 4
Pohjolainen S., Portier-Fozzani F., Ragaigne D., 1999a, Proc. Nobeyama Symp. 1998, NRO Report (in press)
Pohjolainen S., Riehokainen A., Valtaoja E., 1999b, Proc. EPS 1999 Meeting, ESA-SP 448 (in press)
Pohjolainen S., Urpo S., 1997, Fifth SOHO Workshop, ESA SP-404, 619
Portier-Fozzani F., et al., 1996, PASP Conf. Ser. 111, 402
Portier-Fozzani F., 1999, Ph.D. Thesis, University of Nice Sophia Antipolis
Riehokainen A., Urpo S., Valtaoja E., 1998, A&A 333, 741
Shevgaonkar R.K., Kundu M.R., Jackson P.D., 1988, ApJ 329, 982
Shibasaki K., 1997, in Balasubramaniam K.S., Harvey J. and Rabin D. (eds.). Synoptic Solar Physics, ASP Conf. Ser. 140, 373
Tsuneta S., Acton L., Bruner M., Lemen J., Brown W., et al., 1991, Solar Phys. 136, 37
Vršnak B., Pohjolainen S., Urpo S., et al., 1992, Solar Phys. 137, 67

Table 3. April 12, 1996: The radio Quiet Sun Level (QSL) was 7240.0 A/D converter count units (1.000 ± 0.003) in the Metsähovi 87 GHz map at 13:57 − 14:05 UT (Fig. 2). The radio source location is within the one arcmin beam. The Yohkoh SXT map was taken at 13:54:59 UT (Fig. 3), and the SOHO EIT Fe IX/X image at 14:27:41 UT (Fig. 4)

Point	Lat Deg	Long Deg	87 GHz Relative Intensity	Radio structure	EIT structure within 1 arcmin	SXT structure within 1 arcmin
1N	51.1	20.4	1.009 ± 0.003	brightening	LIE	enhanced brightness
2N	43.4	5.1	1.010 ± 0.003	brightening	LID	enhanced brightness
3N	56.8	9.4	1.006 ± 0.003	brightening	LID (He II: near LIE)	near BP
4N	31.3	−5.5	1.004 ± 0.003	brightening	LID	BP
1S	−67.0	5.0	1.017 ± 0.003	brightening	CH (He II: BP)	CH
2S	−55.8	35.0	1.012 ± 0.003	brightening	LID/BP nearby	BP
3S	−58.2	−41.2	1.010 ± 0.003	brightening	LID/BP nearby	enhanced brightness/CH
4S	−61.9	26.9	1.011 ± 0.003	brightening	LID/LIE nearby	enhanced brightness
5S	−47.3	−56.0	1.010 ± 0.003	brightening	LIE	CH/enhanced brightness

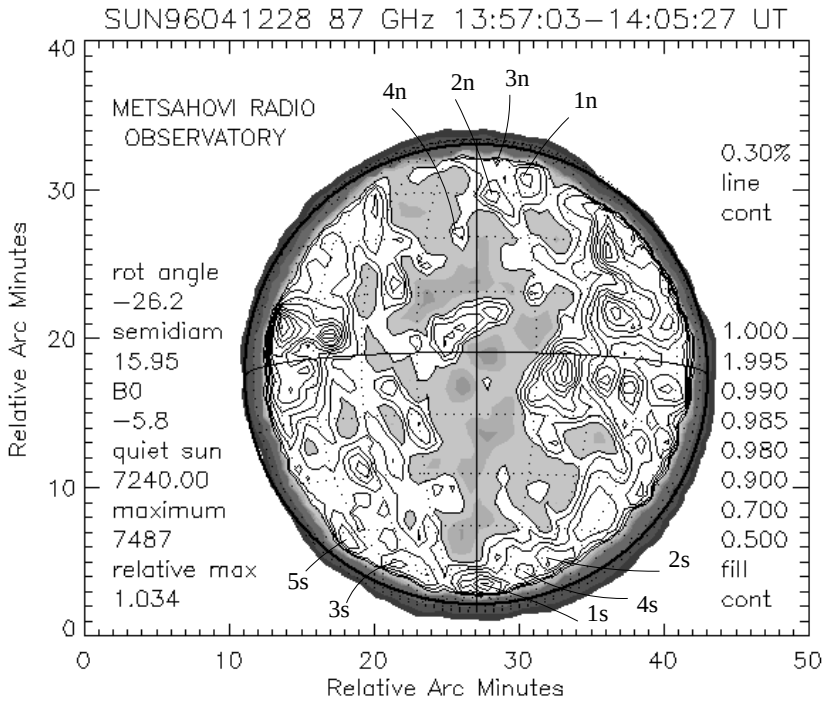

Fig. 2. Solar radio map at 87 GHz (3.5 mm) for April 12, 1996 at 13:57 − 14:05 UT. The greyscale contours (0.5, 0.7, 0.9, 0.98, 0.985, 0.99, and 0.995) represent levels below the quiet Sun. The quiet Sun (level 1.000) is plotted in white color, over which are the enhanced levels plotted in contour lines. The contour line level difference (0.3% of the quiet Sun in this case) is also the flux resolution

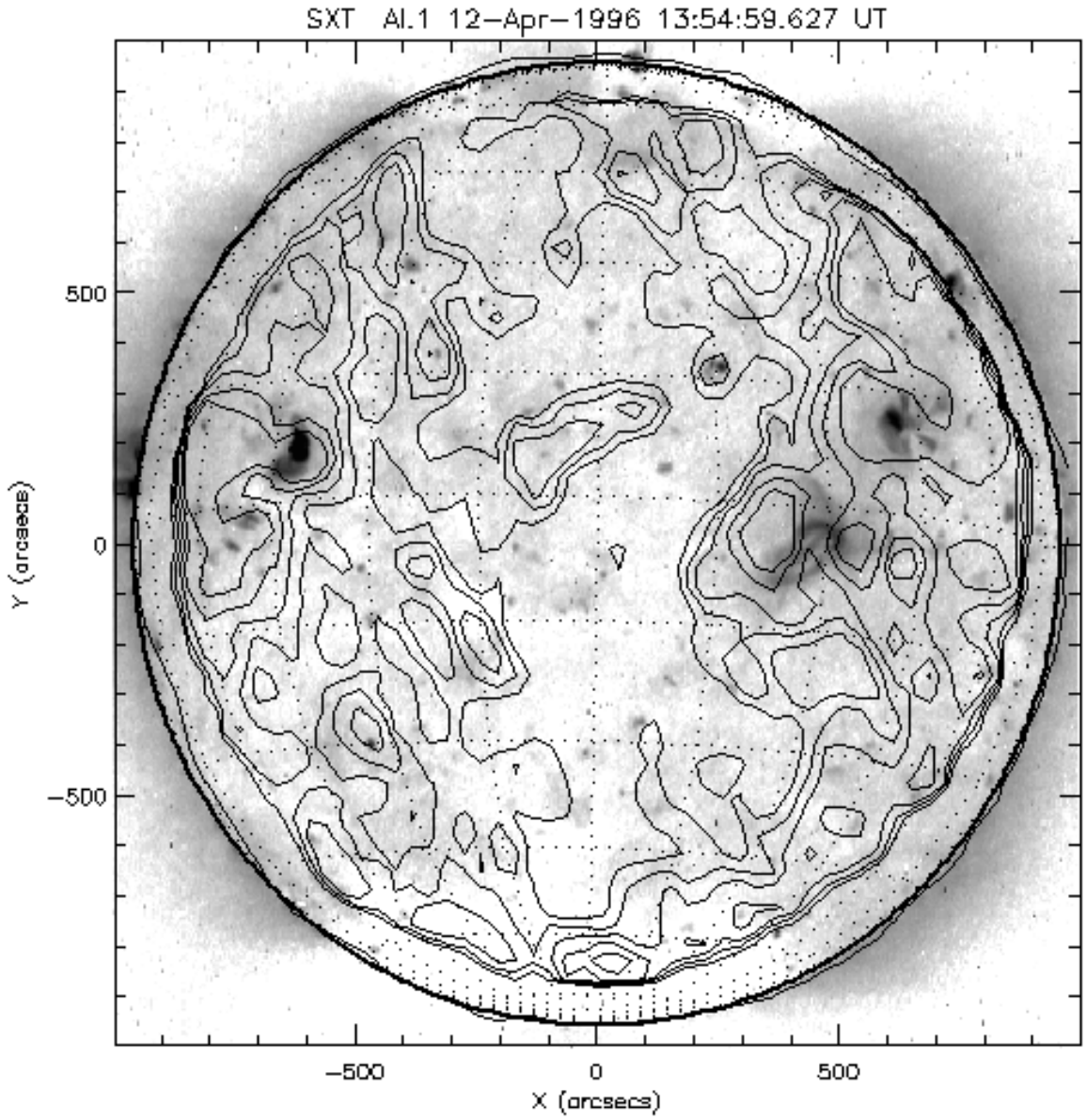

Fig. 3. Yohkoh SXT Al.1 image from April 12, 1996 at 13:54:59 UT (reversed colors). Overplotted are some selected radio contours (above the quiet Sun level only) of the 13:57 − 14:05 UT map

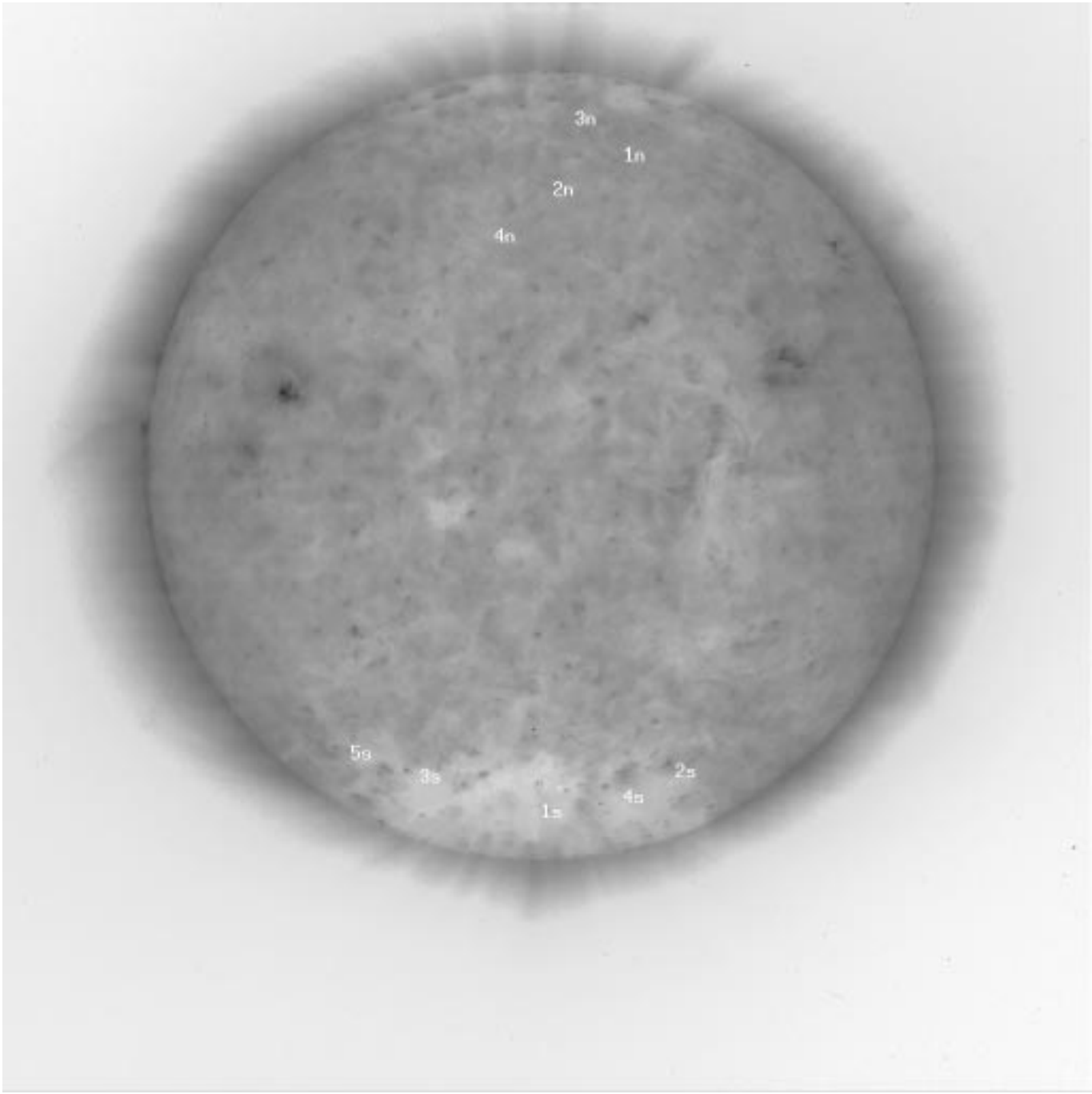

Fig. 4. SOHO/EIT Fe IX/X (171 Å, filter Al+1) image for April 12, 1996 at 14:27:41 UT (reversed colors)

Table 4. April 15, 1996: The radio Quiet Sun Level (QSL) was 7360.0 A/D converter count units (1.000 ± 0.003) in the Metsähovi 87 GHz map at 12:05 − 12:13 UT (Fig. 5). The radio source location is within the one arcmin beam. The Yohkoh SXT map was taken at 11:18:47 UT (Fig. 6), and the SOHO EIT Fe IX/X image at 12:14:16 UT (Fig. 7)

Point	Lat Deg	Long Deg	87 GHz Relative Intensity	Radio structure	EIT structure within 1 arcmin	SXT structure within 1 arcmin
1N	55.5	22.8	1.010 ± 0.003	brightening	LID	enhanced brightness
2N	40.2	4.5	1.007 ± 0.003	brightening	LID/LIE nearby	enhanced brightness
3N	53.2	−13.9	1.004 ± 0.003	brightening	LID/LIE nearby	enhanced/reduced brightness
4N	35.1	−10.1	1.009 ± 0.003	brightening	LIE	enhanced brightness
5N	52.8	33.8	1.011 ± 0.003	brightening	LID	enhanced brightness
6N	31.5	−20.4	1.010 ± 0.003	brightening	LIE	enhanced brightness
7N	53.7	0.4	0.995 ± 0.003	depression	LID	enhanced brightness
8N	45.1	−18.5	0.997 ± 0.003	depression	LIE	reduced brightness
1S	−63.5	−0.3	1.011 ± 0.003	brightening	CH	CH
2S	−64.5	20.6	1.009 ± 0.003	brightening	CH/LIE	CH
3S	−60.7	−36.5	1.014 ± 0.003	brightening	CH/LIE	CH/enhanced brightness
4S	−52.5	43.1	1.010 ± 0.003	brightening	LIE	enhanced brightness
5S	−46.3	48.9	1.010 ± 0.003	brightening	LID/LIE nearby	enhanced brightness
6S	−47.5	6.6	1.007 ± 0.003	brightening	LID/LIE nearby	enhanced brightness

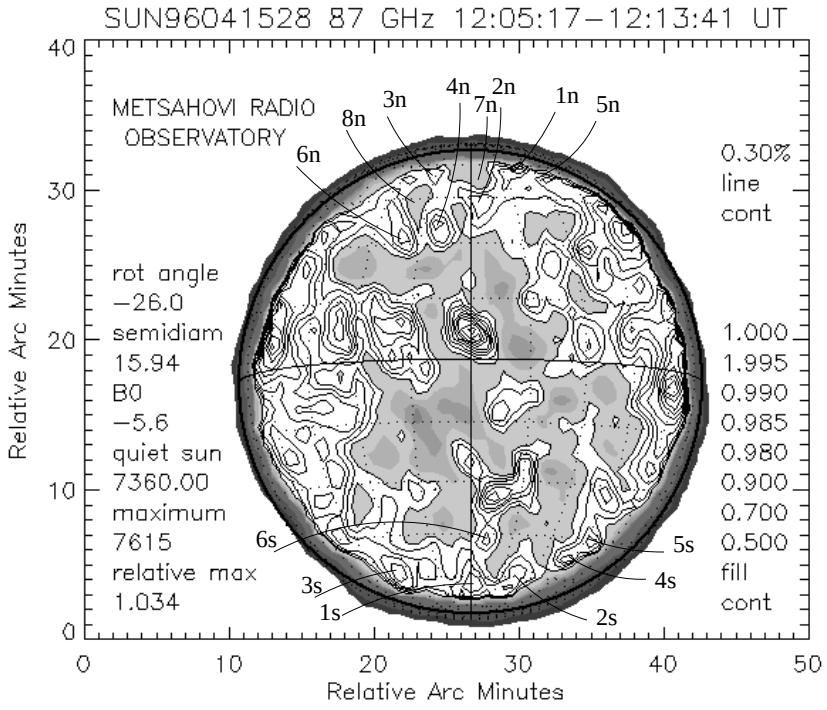

Fig. 5. Solar radio map at 87 GHz (3.5 mm) for April 15, 1996 at 12:05 − 12:13 UT. The greyscale contours (0.5, 0.7, 0.9, 0.98, 0.985, 0.99, and 0.995) represent levels below the quiet Sun. The quiet Sun (level 1.000) is plotted in white color, over which are the enhanced levels plotted in contour lines. The contour line level difference (0.3% of the quiet Sun in this case) is also the flux resolution

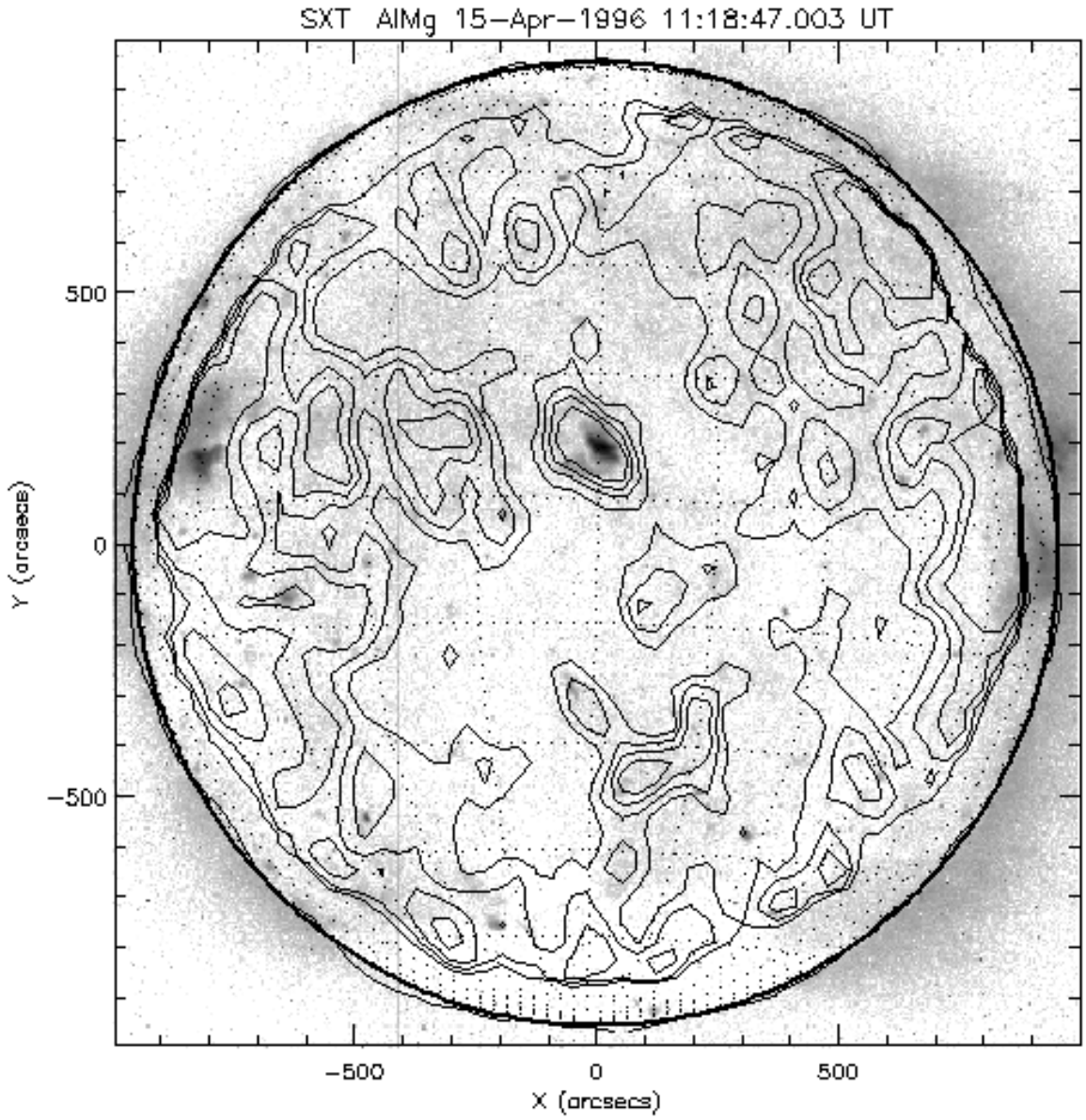

Fig. 6. Yohkoh AlMg image from April 15, 1996 at 11:18:47 UT (reversed colors). Overplotted are some selected radio contours (above the quiet Sun level only) of the 12:05 − 12:13 UT map

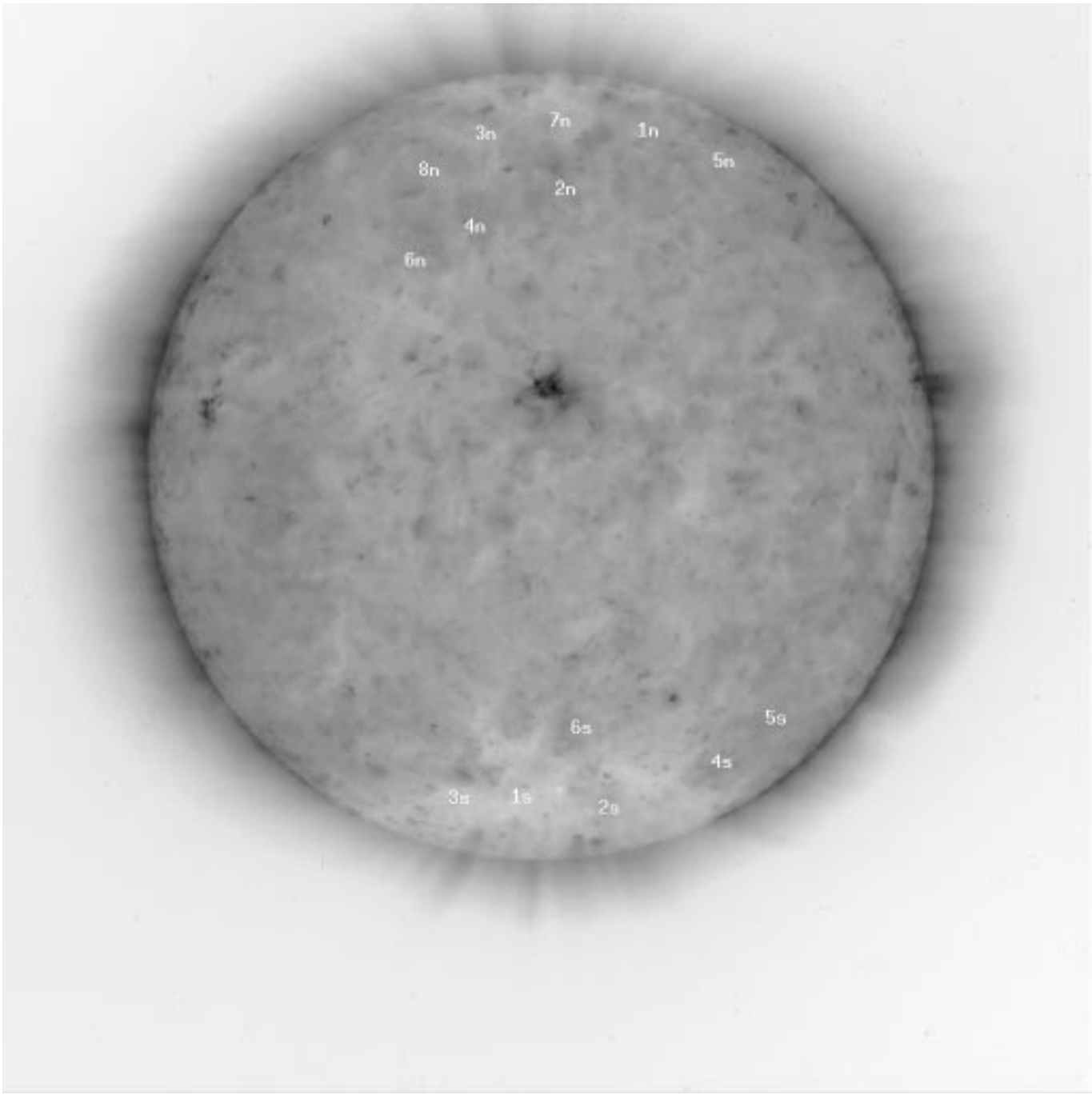

Fig. 7. SOHO/EIT Fe IX/X (171 Å, filter Al+1) image for April 15, 1996 at 12:14:16 UT (reversed colors)

Table 5. August 9, 1996: The radio Quiet Sun Level (QSL) was 5380.0 A/D converter count units (1.000 ± 0.003) in the Metsähovi 87 GHz map at 07:23 − 07:32 UT (Fig. 8). The radio source location is within the one arcmin beam. The Yohkoh SXT map was taken at 07:00:00 UT (Fig. 9), and the SOHO EIT Fe XII image at 07:34:25 UT (Fig. 10)

Point	Lat Deg	Long Deg	87 GHz Relative Intensity	Radio structure	EIT structure within 1 arcmin	SXT structure within 1 arcmin
1N	70.1	16.7	1.015 ± 0.003	brightening	CH	CH
2N	62.1	−27.0	1.019 ± 0.003	brightening	LID/LIE	CH
3N	52.2	3.9	1.013 ± 0.003	brightening	LID/LIE nearby	enhanced brightness
4N	47.4	−42.2	1.013 ± 0.003	brightening	LID	CH/enhanced brightness
5N	58.4	49.1	1.010 ± 0.003	brightening	LIE	enhanced brightness
6N	42.4	−16.7	0.986 ± 0.003	depression	LID	CH
7N	42.5	12.5	0.989 ± 0.003	depression	LID	quiet Sun
8N	37.6	1.7	0.988 ± 0.003	depression	LID	quiet Sun
1S	−52.0	−9.4	1.013 ± 0.003	brightening	LIE	enhanced brightness
2S	−42.4	42.8	1.021 ± 0.003	brightening	BP/LID nearby	BP nearby
3S	−34.9	−9.2	0.986 ± 0.003	depression	LID	reduced brightness

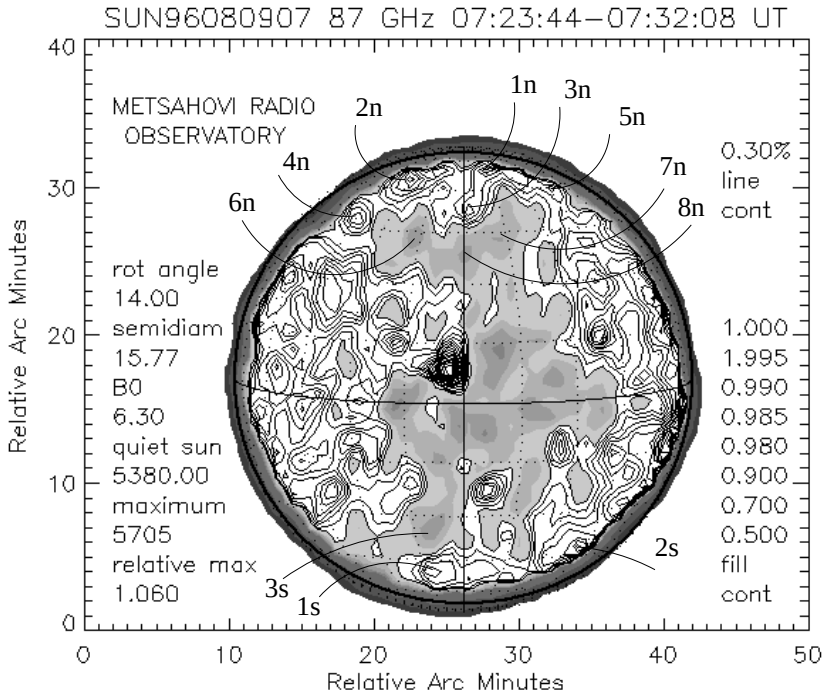

Fig. 8. Solar radio map at 87 GHz (3.5 mm) for August 09, 1996 at 07:23 − 07:32 UT. The greyscale contours (0.5, 0.7, 0.9, 0.98, 0.985, 0.99, and 0.995) represent levels below the quiet Sun. The quiet Sun (level 1.000) is plotted in white color, over which are the enhanced levels plotted in contour lines. The contour line level difference (0.3% of the quiet Sun in this case) is also the flux resolution

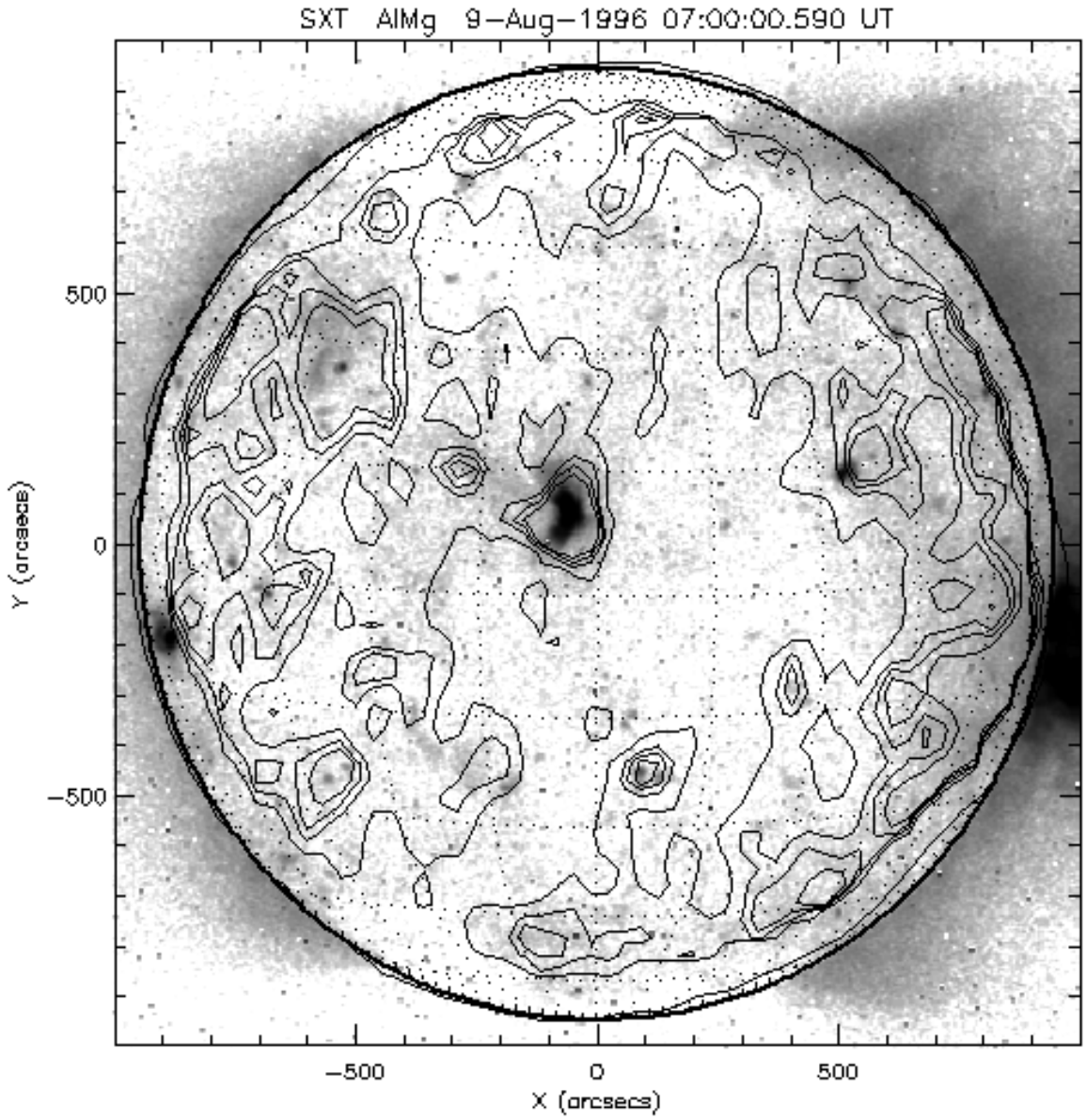

Fig. 9. Yohkoh SXT AlMg image from August 09, 1996 at 07:00:00 UT (reversed colors). Overplotted are some selected radio contours (above the quiet Sun level only) of the 07:23 − 07:32 UT map

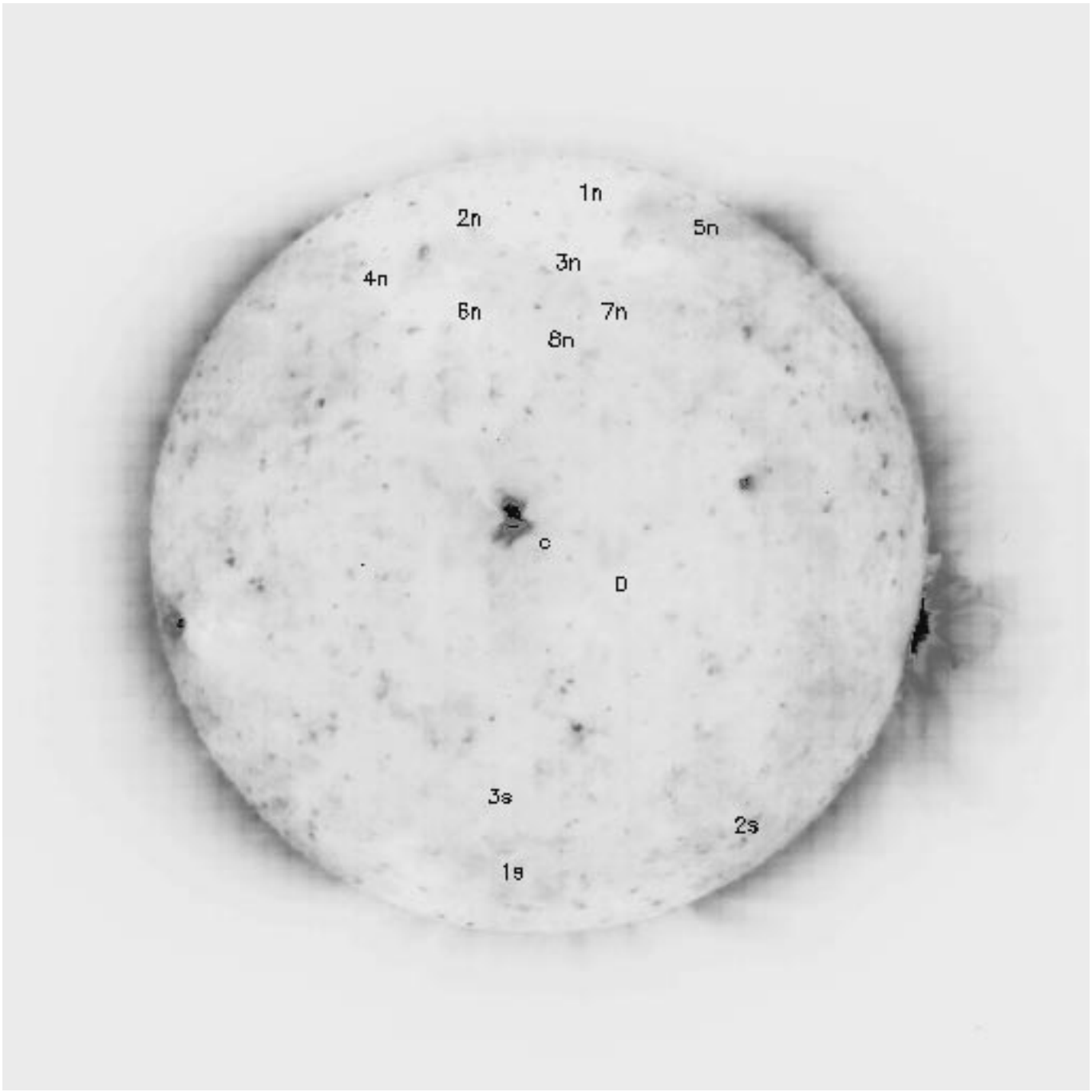

Fig. 10. SOHO/EIT Fe XII (195 Å, filter Clear) image for August 09, 1996 at 07:34:25 UT (reversed colors)

Table 6. August 13, 1996: The radio Quiet Sun Level (QSL) was 5950.0 A/D converter count units (1.000 ± 0.003) in the Metsähovi 87 GHz map at 12:31 − 12:39 UT (Fig. 11). The radio source location is within the one arcmin beam. The Yohkoh SXT map was taken at 12:39:53 UT (Fig. 12), and the SOHO EIT Fe IX/X image at 12:30:13 UT (Fig. 13)

Point	Lat Deg	Long Deg	87 GHz Relative Intensity	Radio structure	EIT structure within 1 arcmin	SXT structure within 1 arcmin
1N	64.7	−6.9	1.013 ± 0.003	brightening	BP or PP	BP
2N	68.5	21.6	1.014 ± 0.003	brightening	PP	CH
3N	64.3	47.8	1.010 ± 0.003	brightening	PP	CH
4N	55.5	50.8	1.005 ± 0.003	brightening	LID/LIE	CH
5N	52.4	5.1	0.989 ± 0.003	depression	LID/LIE	CH
1S	−45.2	−26.3	1.016 ± 0.003	brightening	LIE	enhanced brightness
2S	−40.1	−41.3	1.014 ± 0.003	brightening	LIE	reduced brightness
3S	−29.8	−22.9	1.011 ± 0.003	brightening	LID	enhanced brightnes
4S	−42.9	−1.6	1.011 ± 0.003	brightening	LID/BP nearby	enhanced brightness
5S	−50.5	35.7	1.006 ± 0.003	brightening	LIE	reduced brightness
6S	−53.1	13.6	0.992 ± 0.003	depression	CH	CH
7S	−38.0	−12.4	0.998 ± 0.003	depression	LIE	enhanced brightness

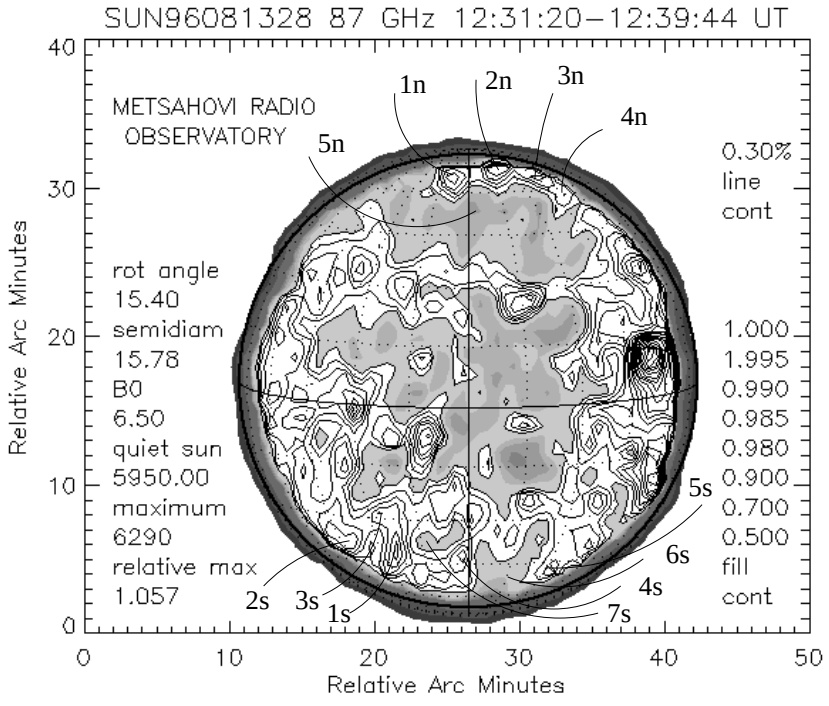

Fig. 11. Solar radio map at 87 GHz (3.5 mm) for August 13, 1996 at 12:31 − 12:39 UT. The greyscale contours (0.5, 0.7, 0.9, 0.98, 0.985, 0.99, and 0.995) represent levels below the quiet Sun. The quiet Sun (level 1.000) is plotted in white color, over which are the enhanced levels plotted in contour lines. The contour line level difference (0.3% of the quiet Sun in this case) is also the flux resolution

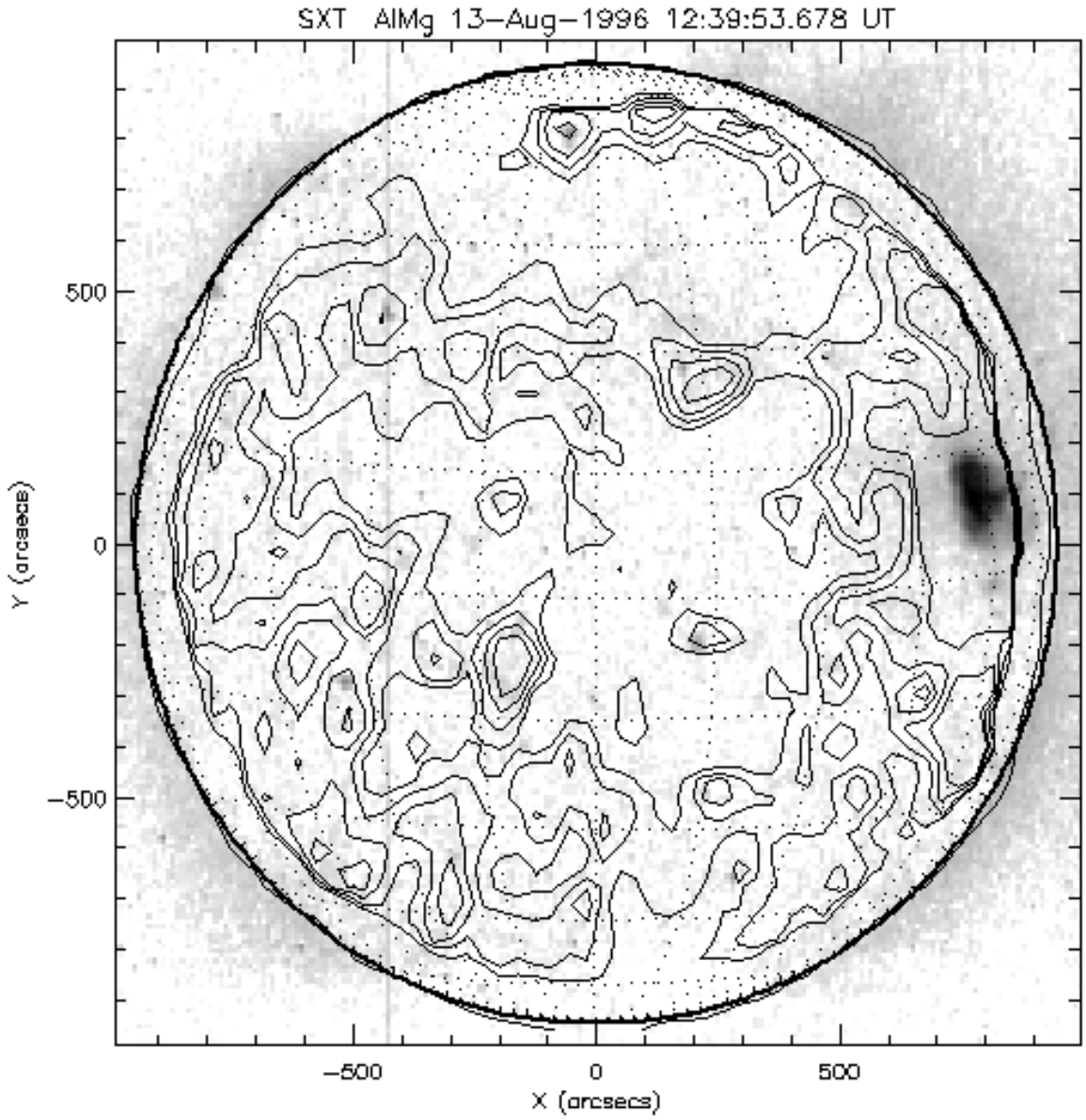

Fig. 12. Yohkoh SXT AlMg image from August 13, 1996 at 12:39:53 UT (reversed colors). Overplotted are some selected radio contours (above the quiet Sun level only) of the 12:31 − 12:39 UT map

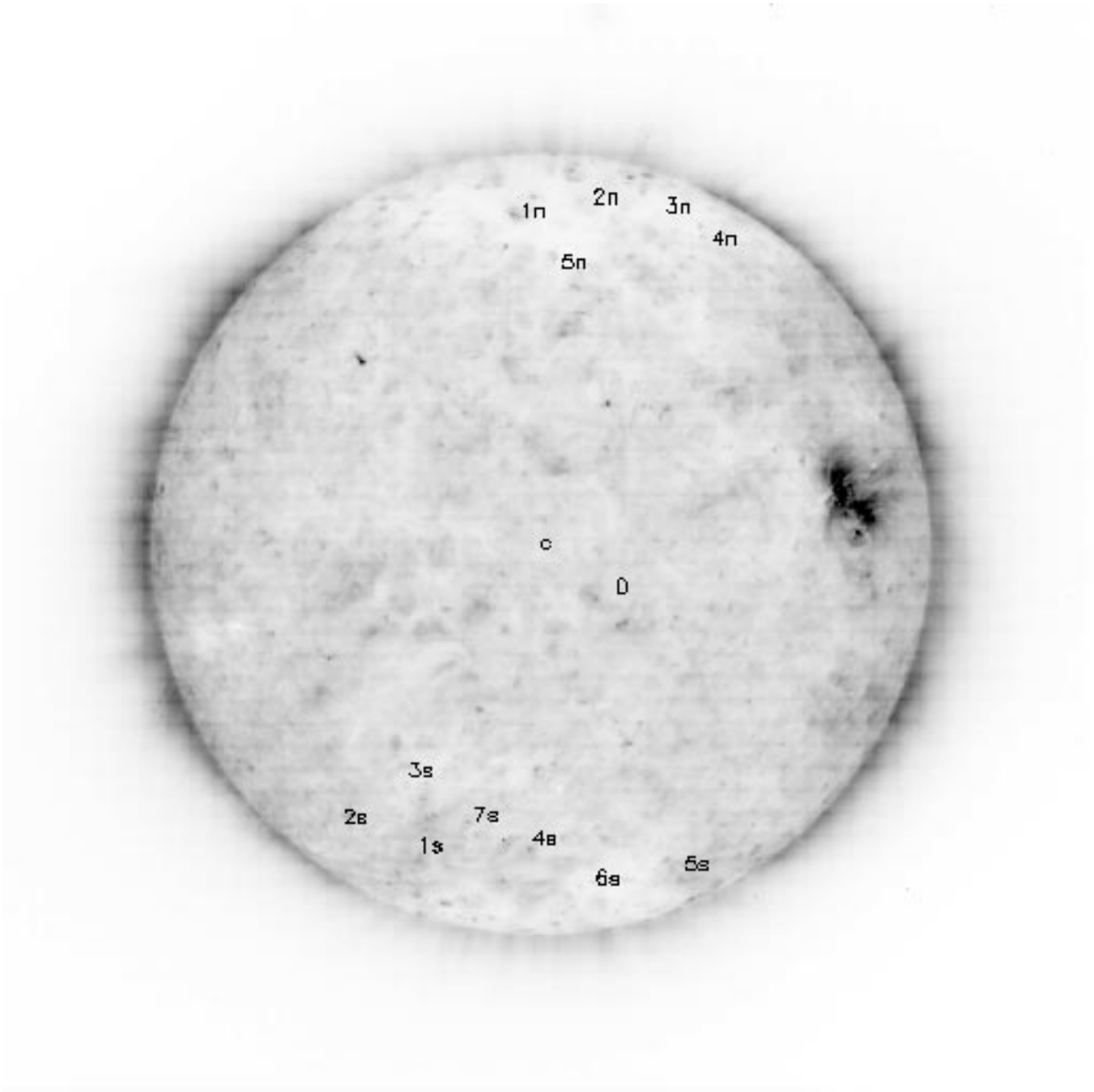

Fig. 13. SOHO/EIT Fe IX/X (171 Å, filter Clear) image for August 13, 1996 at 12:30:13 UT (reversed colors)

Table 7. August 14, 1996: The radio Quiet Sun Level (QSL) was 1985.0 A/D converter count units (1.000 ± 0.003) in the Metsähovi 87 GHz map at 12:55 − 13:03 UT (Fig. 14). The radio source location is within the one arcmin beam. The Yohkoh SXT map was taken at 12:39:41 UT (Fig. 15), and the SOHO EIT Fe IX/X image at 12:30:13 UT (Fig. 16)

Point	Lat Deg	Long Deg	87 GHz Relative Intensity	Radio structure	EIT structure within 1 arcmin	SXT structure within 1 arcmin
1N	67.5	30.0	1.018 ± 0.003	brightening	LIE	CH
2N	67.4	−11.5	1.015 ± 0.003	brightening	PP?	CH
3N	49.6	−47.0	1.006 ± 0.003	brightening	LID	enhanced brightness
4N	51.3	14.8	0.987 ± 0.003	depression	LID	CH
1S	−39.8	−9.4	1.021 ± 0.003	brightening	LID/BP nearby	BP
2S	−40.9	12.7	1.015 ± 0.003	brightening	LID	enhanced brightness
3S	−25.3	31.3	1.018 ± 0.003	brightening	LIE	enhanced brightness
4S	−35.1	−32.8	1.013 ± 0.003	brightening	LID/BP nearby	enhanced brightness
5S	−50.9	24.9	0.997 ± 0.003	depression	CH	CH
6S	−26.3	3.1	0.997 ± 0.003	depression	LID	quiet Sun

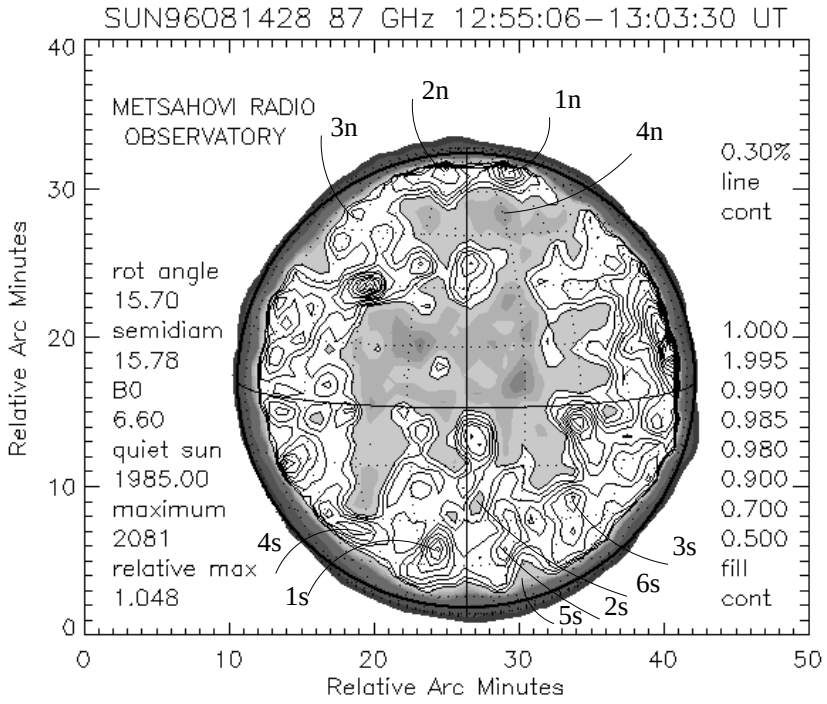

Fig. 14. Solar radio map at 87 GHz (3.5 mm) for August 14, 1996 at 12:55 − 13:03 UT. The greyscale contours (0.5, 0.7, 0.9, 0.98, 0.985, 0.99, and 0.995) represent levels below the quiet Sun. The quiet Sun (level 1.000) is plotted in white color, over which are the enhanced levels plotted in contour lines. The contour line level difference (0.3% of the quiet Sun in this case) is also the flux resolution

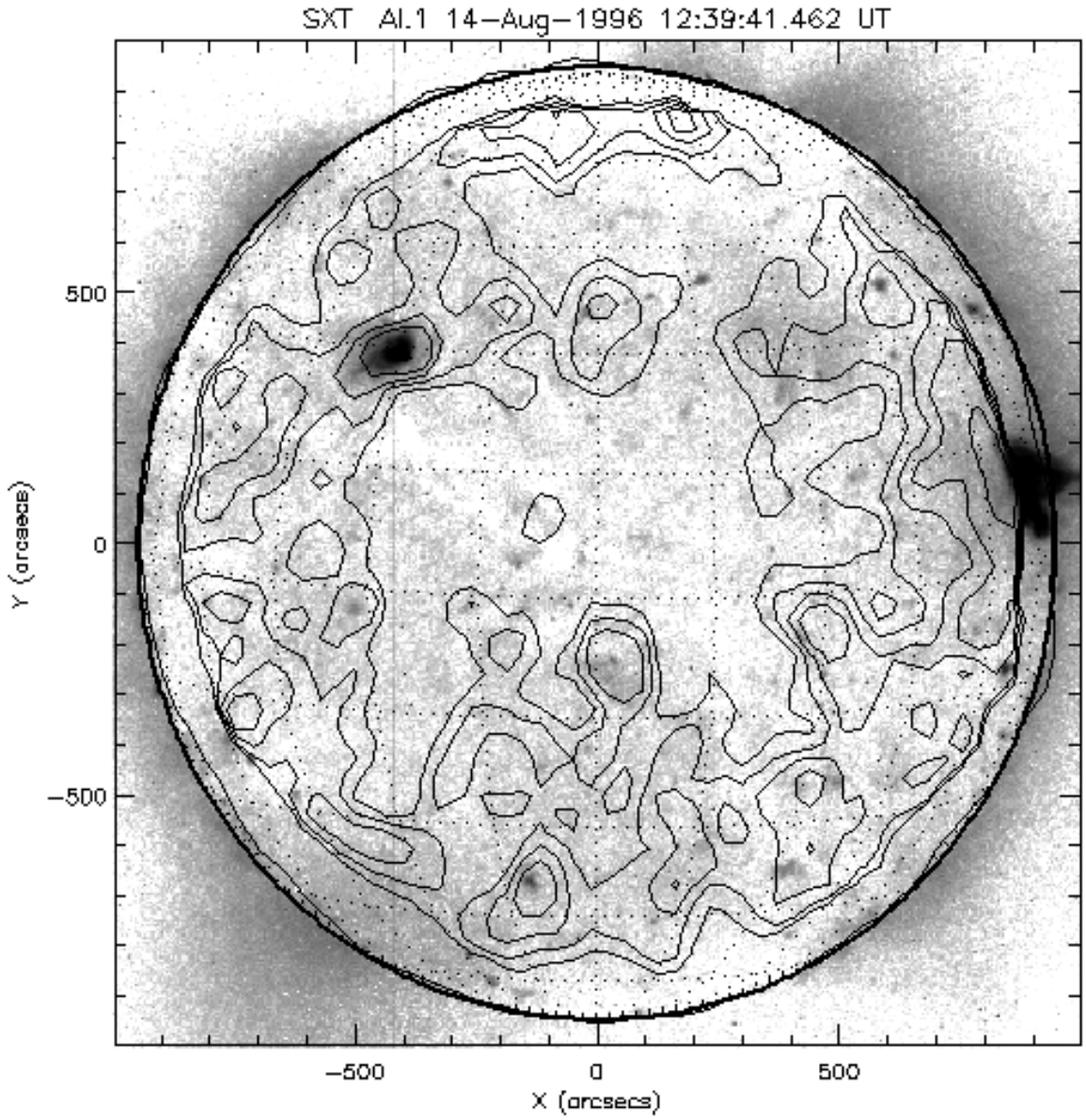

Fig. 15. Yohkoh SXT Al.1 image from August 14, 1996 at 12:39:41 UT (reversed colors). Overplotted are some selected radio contours (above the quiet Sun level only) of the 12:55 − 13:03 UT map

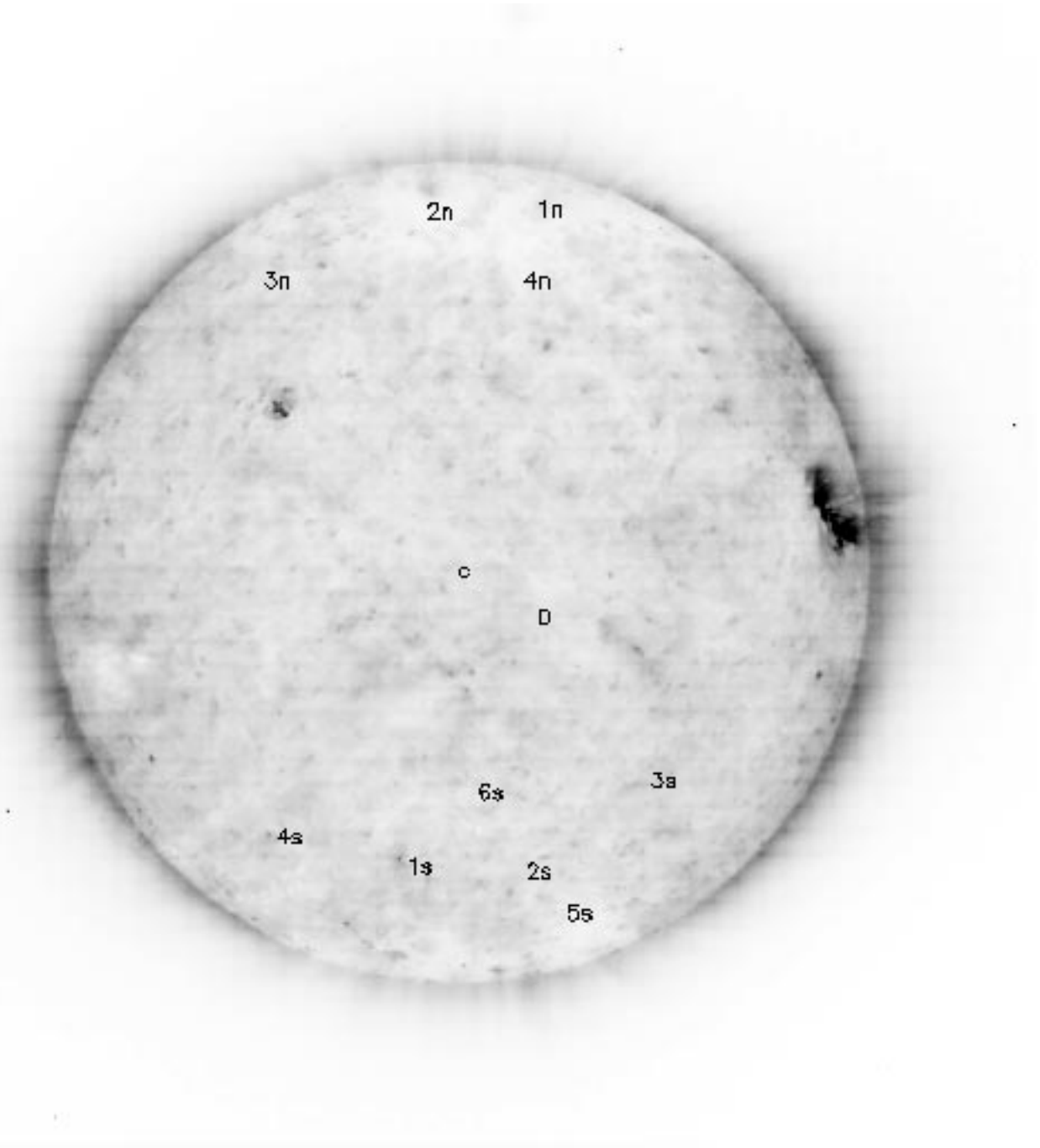

Fig. 16. SOHO/EIT Fe IX/X (171 Å, filter Clear) image for August 14, 1996 at 12:30:13 UT (reversed colors)

Table 8. May 20, 1997: The radio Quiet Sun Level (QSL) was 6910.0 A/D converter count units (1.000 ± 0.005) in the Metsähovi 87 GHz map at 13:03 − 13:12 UT (Fig. 17). The radio source location is within the one arcmin beam. The Yohkoh SXT map was taken at 13:15:13 UT (Fig. 18), and the SOHO EIT Fe IX/X image at 13:00:13 UT (Fig. 19)

Point	Lat Deg	Long Deg	87 GHz Relative Intensity	Radio structure	EIT structure within 1 arcmin	SXT structure within 1 arcmin
1N	58.7	−2.8	1.006 ± 0.005	brightening	CH/LIE	enhanced brightness
2N	47.8	−10.2	1.001 ± 0.005	brightening	LID/LIE	enhanced brightness
3N	44.4	26.7	1.011 ± 0.005	brightening	LID/LIE	enhanced brightness
4N	53.6	−22.9	0.997 ± 0.005	depression	LID/LIE	quiet Sun/CH
5N	54.8	18.1	0.993 ± 0.005	depression	LID/LIE	CH
6N	33.7	10.7	0.988 ± 0.005	depression	LID	reduced brightness
1S	−47.1	−29.6	1.013 ± 0.005	brightening	LIE	BP?
2S	−59.5	1.2	1.004 ± 0.005	brightening	LIE/LID	CH
3S	−53.3	28.4	1.006 ± 0.005	brightening	LIE	BP?
4S	−41.8	−4.4	1.006 ± 0.005	brightening	LID/LIE	reduced brightness
5S	−50.4	−9.0	0.993 ± 0.005	depression	LID/LIE	reduced brightness
6S	−43.8	28.1	0.997 ± 0.005	depression	LID/LIE nearby	reduced brightness

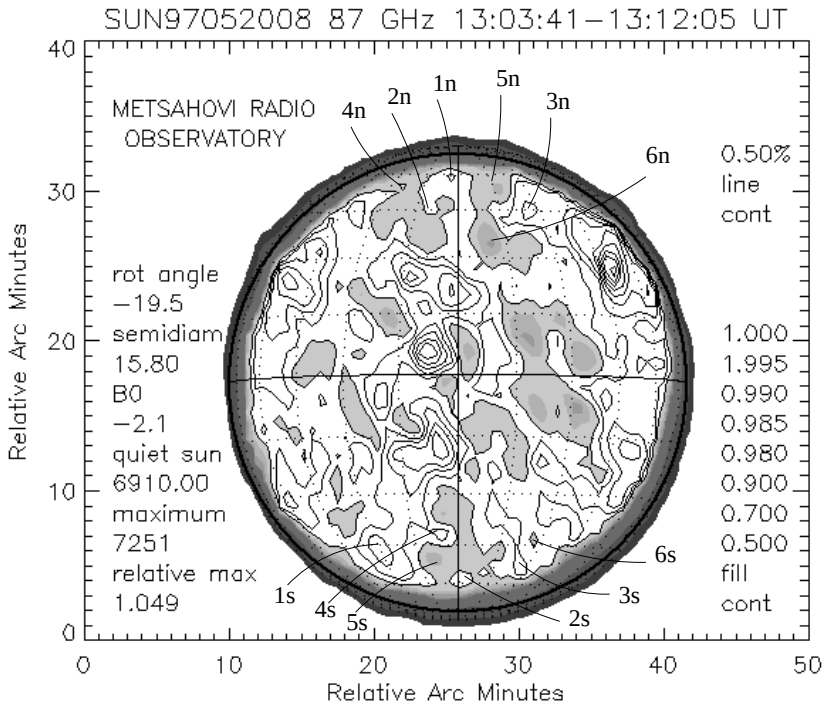

Fig. 17. Solar radio map at 87 GHz (3.5 mm) for May 20, 1997 at 13:03 − 13:12 UT. The greyscale contours (0.5, 0.7, 0.9, 0.98, 0.985, 0.99, and 0.995) represent levels below the quiet Sun. The quiet Sun (level 1.000) is plotted in white color, over which are the enhanced levels plotted in contour lines. The contour line level difference (0.5% of the quiet Sun in this case) is also the flux resolution

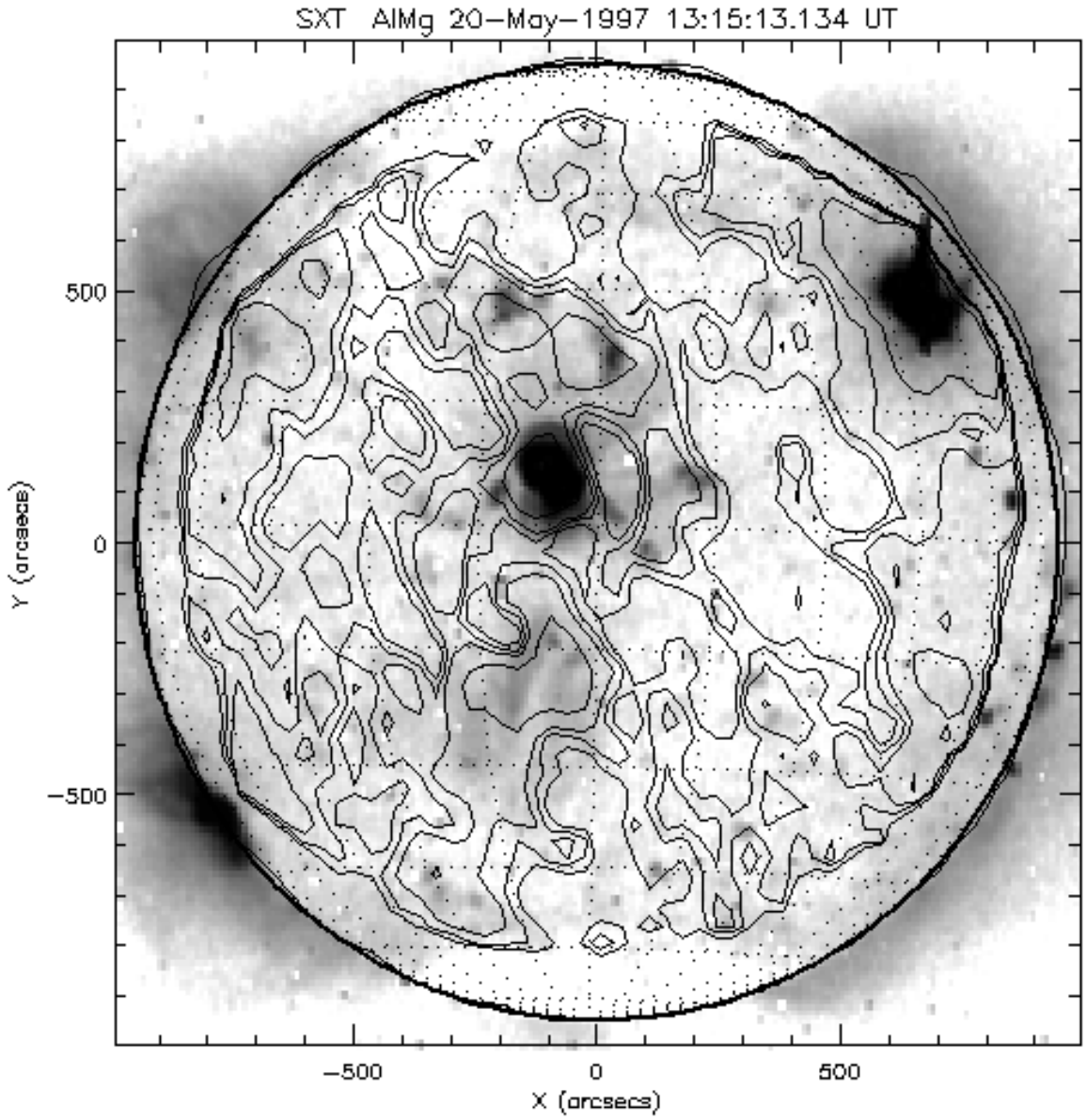

Fig. 18. Yohkoh SXT AlMg image from May 20, 1997 at 13:15:13 UT (reversed colors). Overplotted are some selected radio contours (above the quiet Sun level only) of the 13:03 − 13:12 UT map

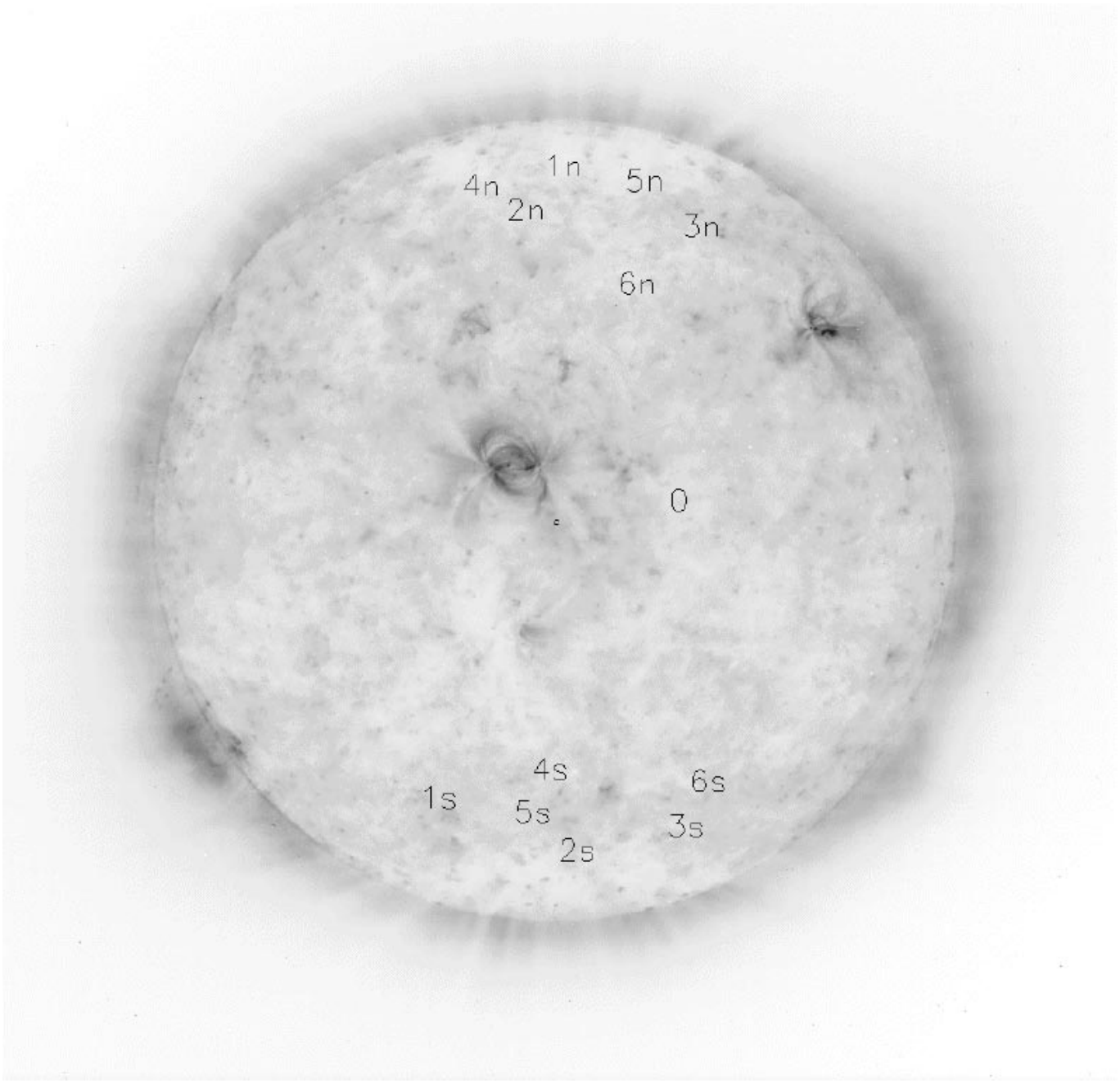

Fig. 19. SOHO/EIT Fe IX/X (171 Å, filter Clear) image for May 20, 1997 at 13:00:13 UT (reversed colors)

Table 9. August 8, 1997: The radio Quiet Sun Level (QSL) was 5350.0 A/D converter count units (1.000 ± 0.004) in the Metsähovi 87 GHz map at 11:30 − 11:39 UT (Fig. 20). The radio source location is within the one arcmin beam. The Yohkoh SXT map was taken at 11:03:59 UT (Fig. 21), and the SOHO EIT Fe IX/X image at 13:09:46 UT (Fig. 22)

Point	Lat Deg	Long Deg	87 GHz Relative Intensity	Radio structure	EIT structure within 1 arcmin	SXT structure within 1 arcmin
1N	65.6	38.9	1.009 ± 0.004	brightening	CH	CH/quiet Sun
2N	66.7	−8.3	1.004 ± 0.004	brightening	CH	CH
3N	51.8	43.7	1.005 ± 0.004	brightening	LID/LIE	enhanced brightness
4N	55.7	−39.9	1.007 ± 0.004	brightening	LIE/BP	enhanced brightness
5N	47.1	−22.7	1.003 ± 0.004	brightening	LIE/BP	enhanced brightness
6N	40.1	−10.9	1.002 ± 0.004	brightening	LID	CH/quiet Sun
7N	52.2	−9.5	0.982 ± 0.004	depression	LID/LIE	CH
1S	−37.5	−43.7	1.032 ± 0.004	brightening	LIE	enhanced brightness
2S	−30.9	−23.6	1.038 ± 0.004	brightening	LID/LIE nearby	AR
3S	−52.4	2.8	1.009 ± 0.004	brightening	LID/LIE	enhanced brightness
4S	−22.8	26.3	1.040 ± 0.004	brightening	AR	AR
5S	−21.0	−19.5	1.036 ± 0.004	brightening	AR	AR
6S	−35.2	−6.2	0.998 ± 0.004	depression	LID	reduced brightness

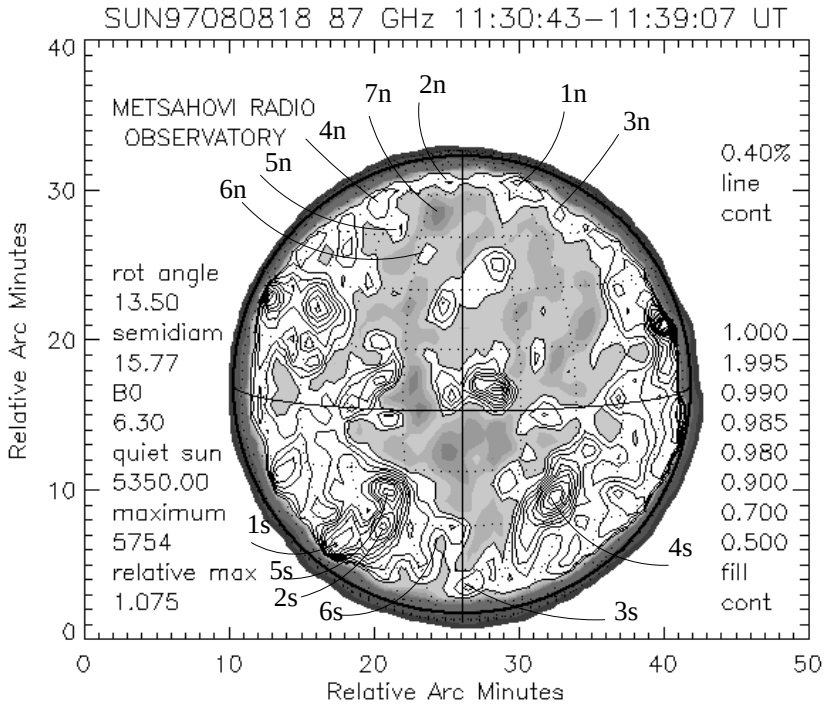

Fig. 20. Solar radio map at 87 GHz (3.5 mm) for August 8, 1997 at 11:30 − 11:39 UT. The greyscale contours (0.5, 0.7, 0.9, 0.98, 0.985, 0.99, and 0.995) represent levels below the quiet Sun. The quiet Sun (level 1.000) is plotted in white color, over which are the enhanced levels plotted in contour lines. The contour line level difference (0.4% of the quiet Sun in this case) is also the flux resolution

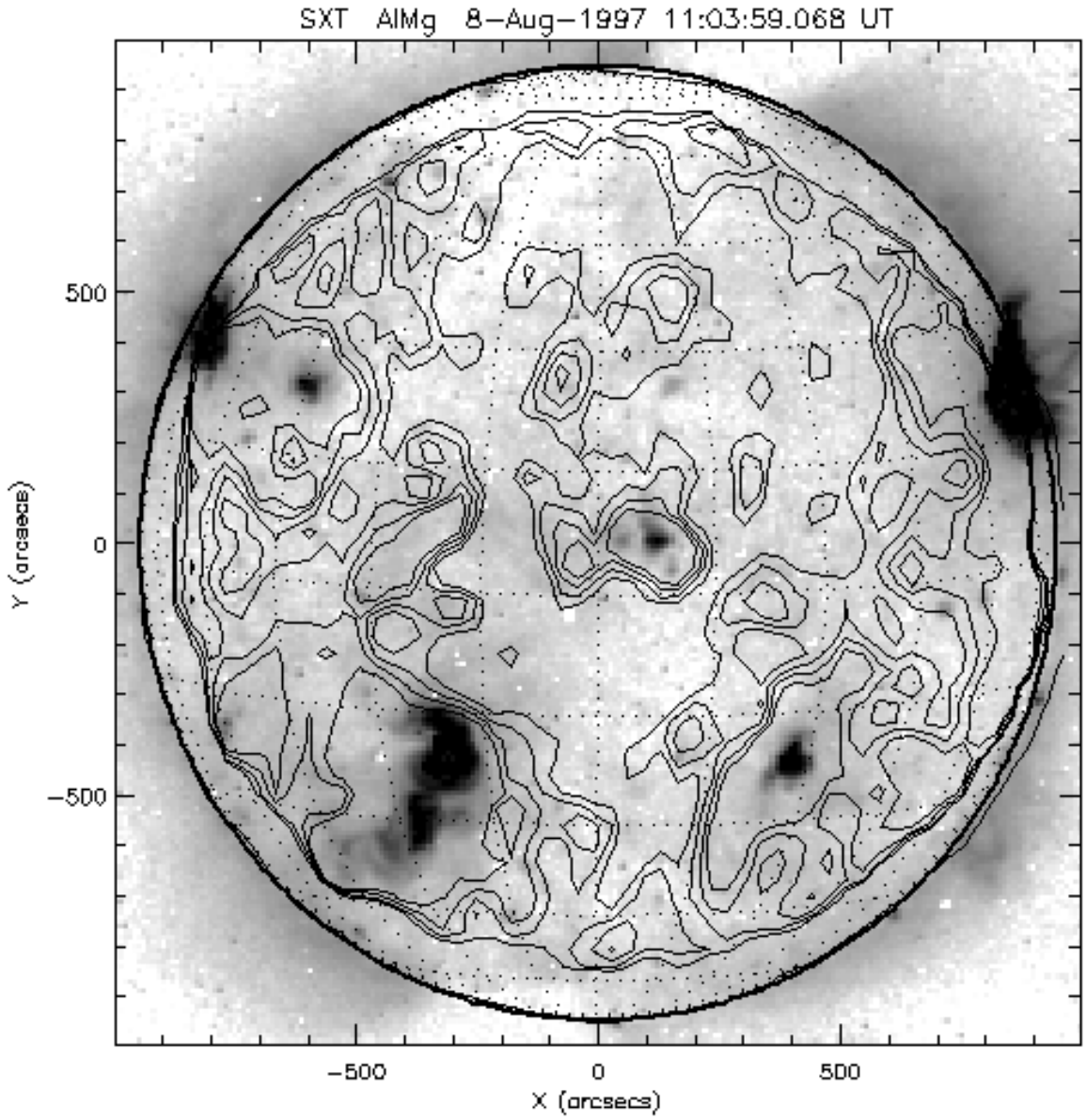

Fig. 21. Yohkoh SXT AlMg image from August 8, 1997 at 11:03:59 UT (reversed colors). Overplotted are some selected radio contours (above the quiet Sun level only) of the 11:30 − 11:39 UT map

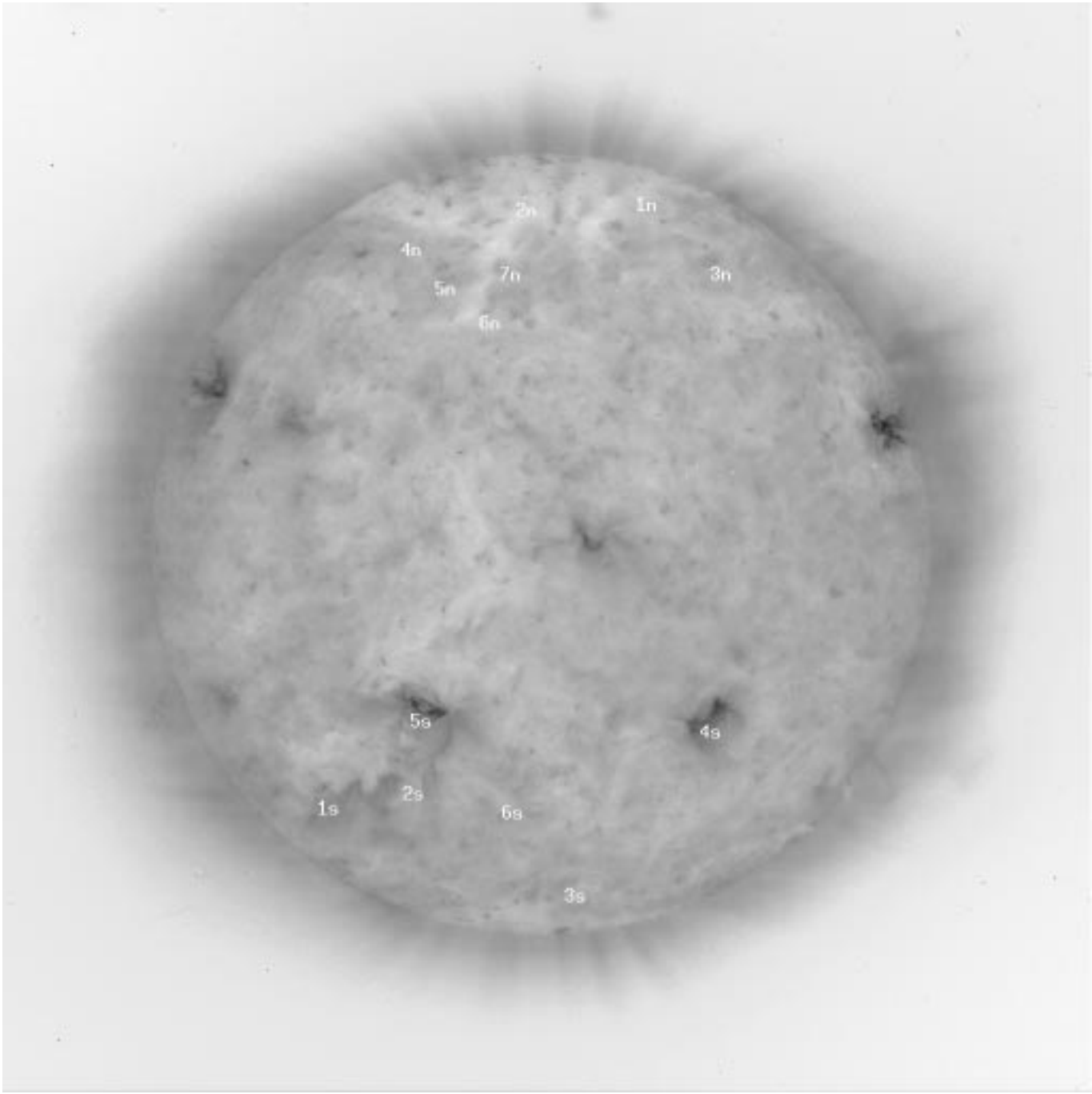

Fig. 22. SOHO/EIT Fe IX/X (171 Å, filter Clear) image for August 8, 1997 at 13:09:46 UT (reversed colors)

Table 10. August 27, 1997: The radio Quiet Sun Level (QSL) was 4560.0 A/D converter count units (1.000 ± 0.005) in the Metsähovi 87 GHz at 12:13 − 12:22 UT (Fig. 23). The radio source location is within the one arcmin beam. The Yohkoh SXT map was taken at 12:53:45 UT (Fig. 24), and the SOHO EIT Fe IX/X image at 13:01:03 UT (Fig. 25)

Point	Lat Deg	Long Deg	87 GHz Relative Intensity	Radio structure	EIT structure within 1 arcmin	SXT structure within 1 arcmin
1N	68.4	−7.1	1.018 ± 0.005	brightening	CH	CH
2N	65.8	−27.2	1.026 ± 0.005	brightening	LIE	enhanced brightness (large loop)
3N	66.9	13.4	1.015 ± 0.005	brightening	CH	CH
4N	62.3	41.5	1.012 ± 0.005	brightening	LID/LIE	CH
5N	56.5	−40.9	1.018 ± 0.005	brightening	LIE	enhanced brightness
6N	55.2	11.1	0.991 ± 0.005	depression	LID	CH
1S	−42.0	27.6	1.025 ± 0.005	brightening	LID/LIE	enhanced brightness
2S	−35.6	40.2	1.024 ± 0.005	brightening	LID	reduced brightness
3S	−48.5	−14.8	1.014 ± 0.005	brightening	LID/LIE nearby	enhanced brightness/CH
4S	−36.6	−2.8	1.014 ± 0.005	brightening	LID/LIE	enhanced brightness
5S	−42.1	−29.1	1.021 ± 0.005	brightening	LID/LIE	enhanced brightness
6S	−31.7	9.1	0.987 ± 0.005	depression	LID	reduced brightness

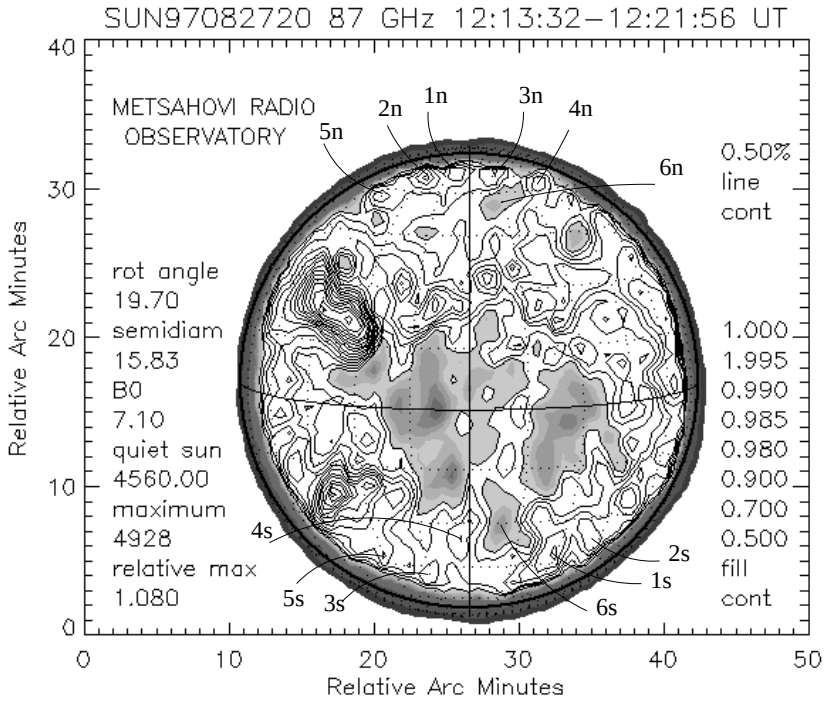

Fig. 23. Solar radio map at 87 GHz (3.5 mm) for August 27, 1997 at 12:13 − 12:22 UT. The greyscale contours (0.5, 0.7, 0.9, 0.98, 0.985, 0.99, and 0.995) represent levels below the quiet Sun. The quiet Sun (level 1.000) is plotted in white color, over which are the enhanced levels plotted in contour lines. The contour line level difference (0.5% of the quiet Sun in this case) is also the flux resolution

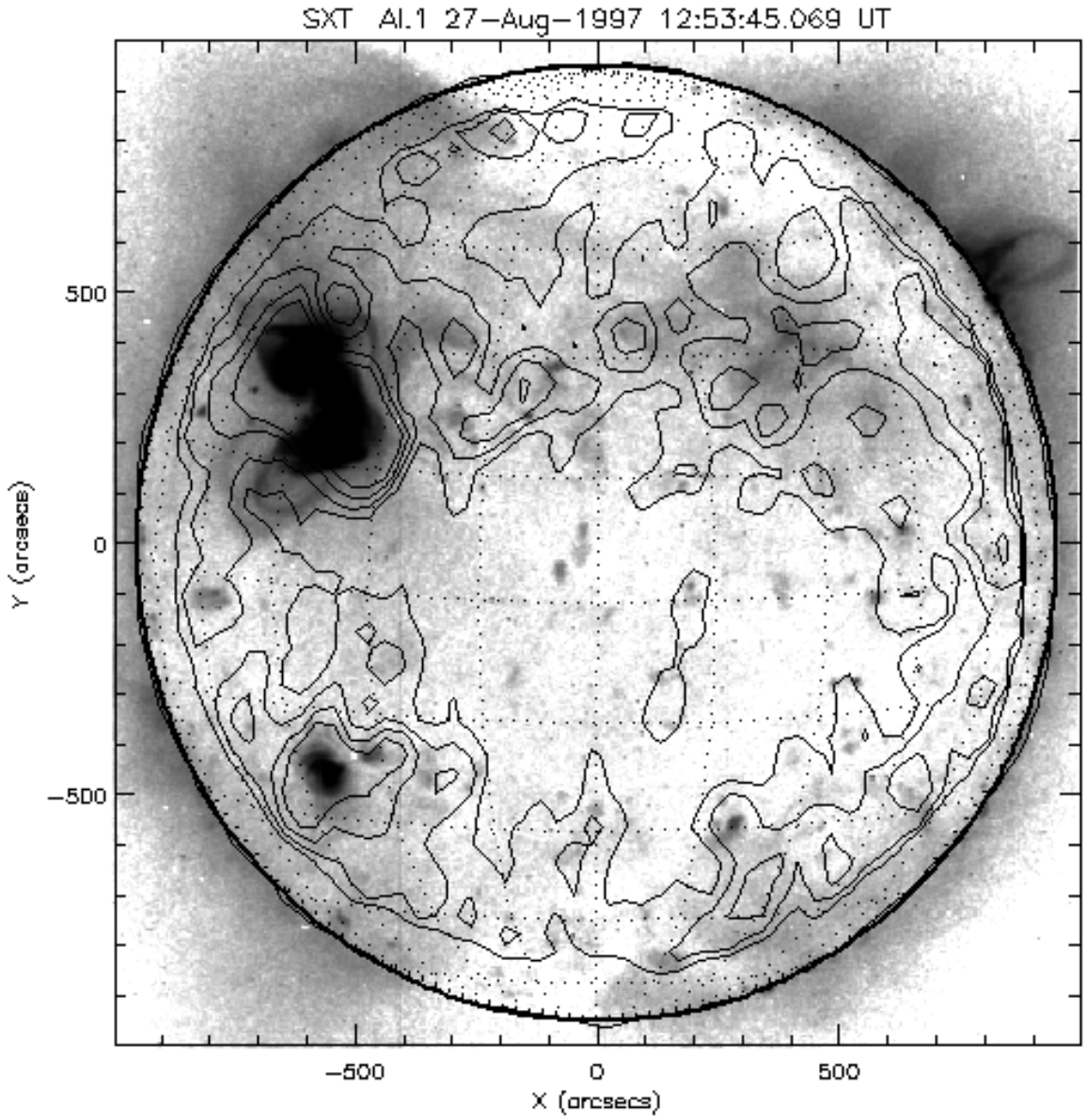

Fig. 24. Yohkoh SXT Al.1 image from August 27, 1997 at 12:53:45 UT (reversed colors). Overplotted are some selected radio contours (above the quiet Sun level only) of the 12:13 − 12:22 UT map

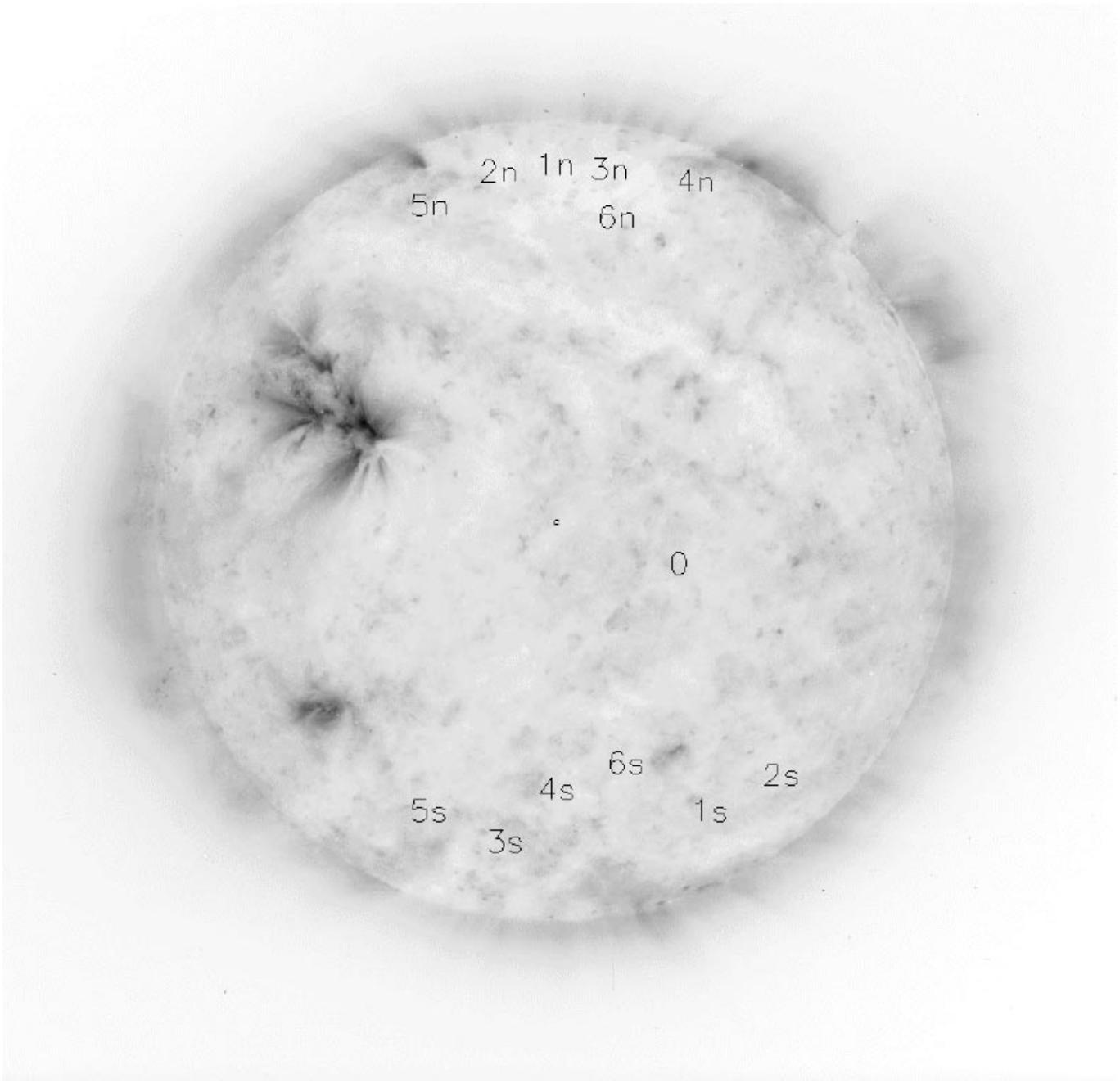

Fig. 25. SOHO/EIT Fe IX/X (171 Å, filter Clear) image for August 27, 1997 at 13:01:03 UT (reversed colors)

Table 11. August 28, 1997: The radio Quiet Sun Level (QSL) was 4480.0 A/D converter count units (1.000 ± 0.005) in the Metsähovi 87 GHz map at 07:16 − 07:24 UT (Fig. 26). The radio source location is within the one arcmin beam. The Yohkoh SXT map was taken at 07:23:28 UT (Fig. 27), and the SOHO EIT He II/Si XI image at 07:18:19 UT (Fig. 28)

Point	Lat Deg	Long Deg	87 GHz Relative Intensity	Radio structure	EIT structure within 1 arcmin	SXT structure within 1 arcmin
1N	64.5	24.3	1.012 ± 0.005	brightening	CH (He II: LIE)	CH
2N	64.3	−10.2	1.023 ± 0.005	brightening	CH	enhanced brightness (large loop)
3N	63.7	−26.9	1.033 ± 0.005	brightening	LID/LIE	enhanced brightness (large loop)
4N	57.6	−40.6	1.026 ± 0.005	brightening	LID/LIE	enhanced brightness (large loop)
5N	54.8	−5.1	1.013 ± 0.005	brightening	LID/BP nearby	enhanced brightness
6N	52.4	20.0	0.992 ± 0.005	depression	LID	reduced brightness
7N	41.1	−3.5	0.996 ± 0.005	depression	LID	reduced brightness
1S	−56.3	22.7	1.006 ± 0.005	brightening	LID/LIE	reduced brightness
2S	−30.4	8.9	1.008 ± 0.005	brightening	LID	enhanced brightness/BP nearby
3S	−25.0	−28.7	1.040 ± 0.005	brightening	AR	AR
4S	−36.5	48.7	1.021 ± 0.005	brightening	LID/LIE nearby	enhanced brightness

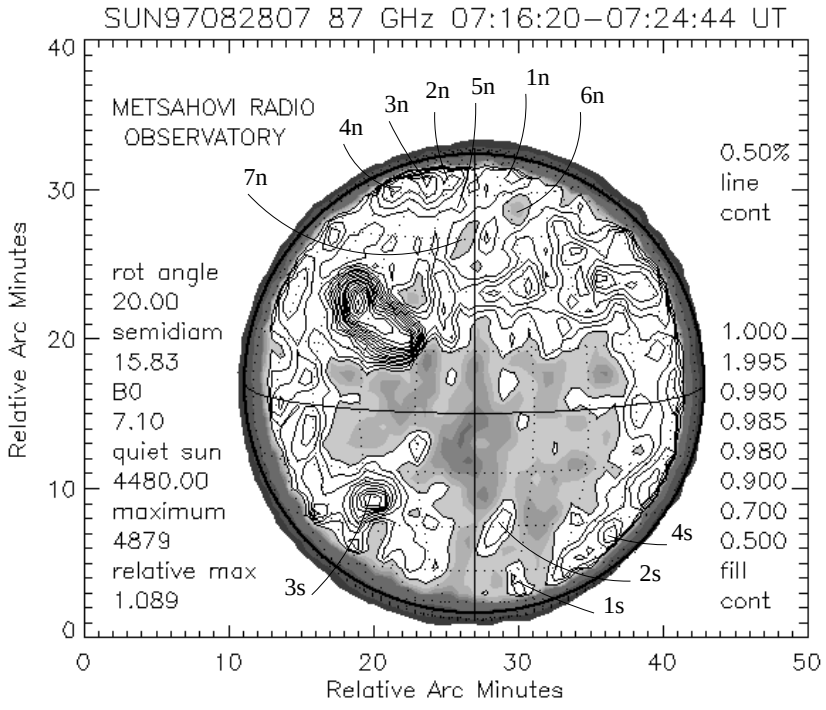

Fig. 26. Solar radio map at 87 GHz (3.5 mm) for August 28, 1997 at 07:16 − 07:24 UT. The greyscale contours (0.5, 0.7, 0.9, 0.98, 0.985, 0.99, and 0.995) represent levels below the quiet Sun. The quiet Sun (level 1.000) is plotted in white color, over which are the enhanced levels plotted in contour lines. The contour line level difference (0.5% of the quiet Sun in this case) is also the flux resolution

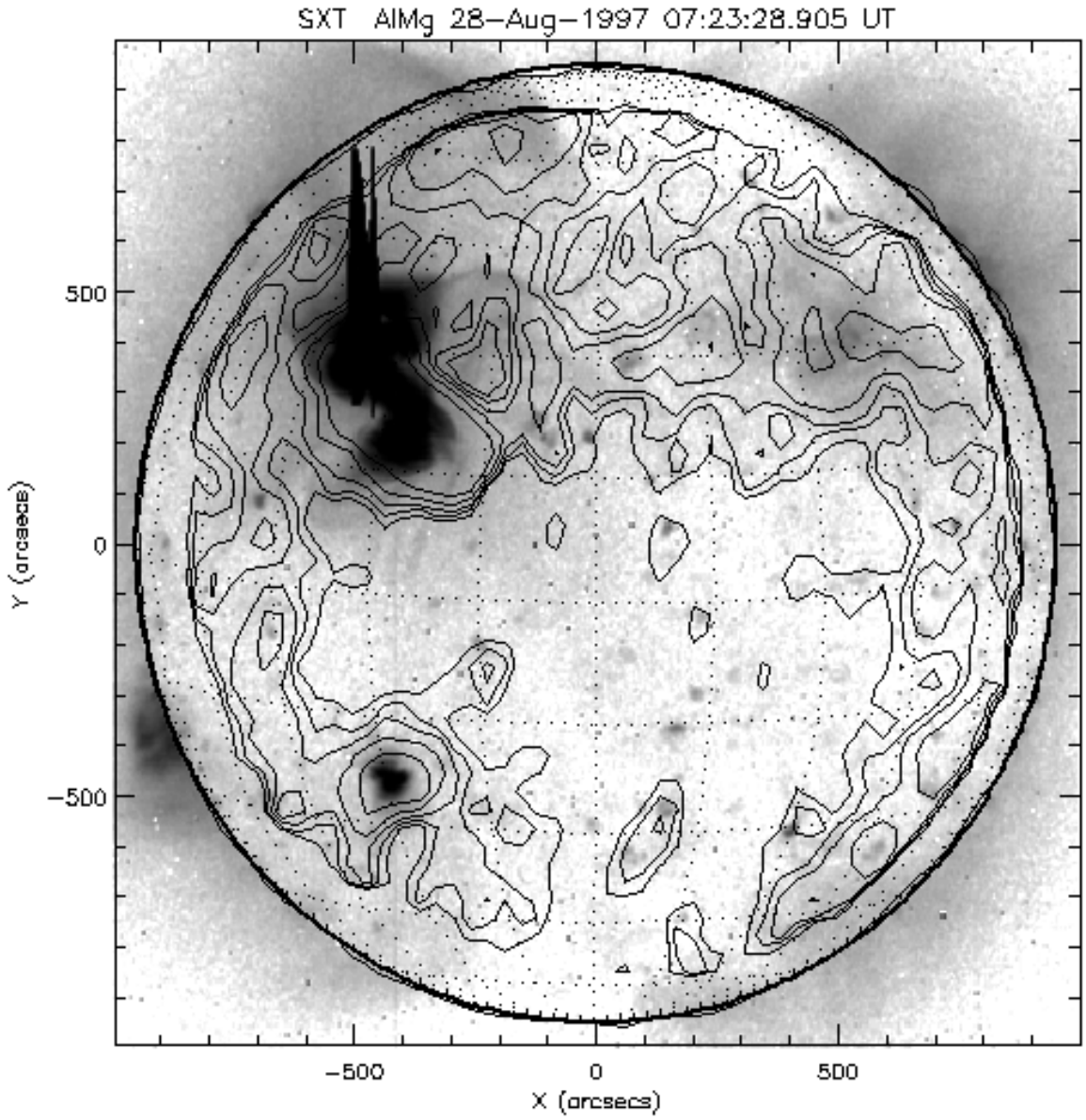

Fig. 27. Yohkoh SXT Al.1 image from August 28, 1997 at 07:23:28 UT (reversed colors). Overplotted are some selected radio contours (above the quiet Sun level only) of the 07:16 − 07:24 UT map

Fig. 28. SOHO/EIT He II (304 Å, filter Clear) image for August 28, 1997 at 07:18:19 UT (reversed colors)

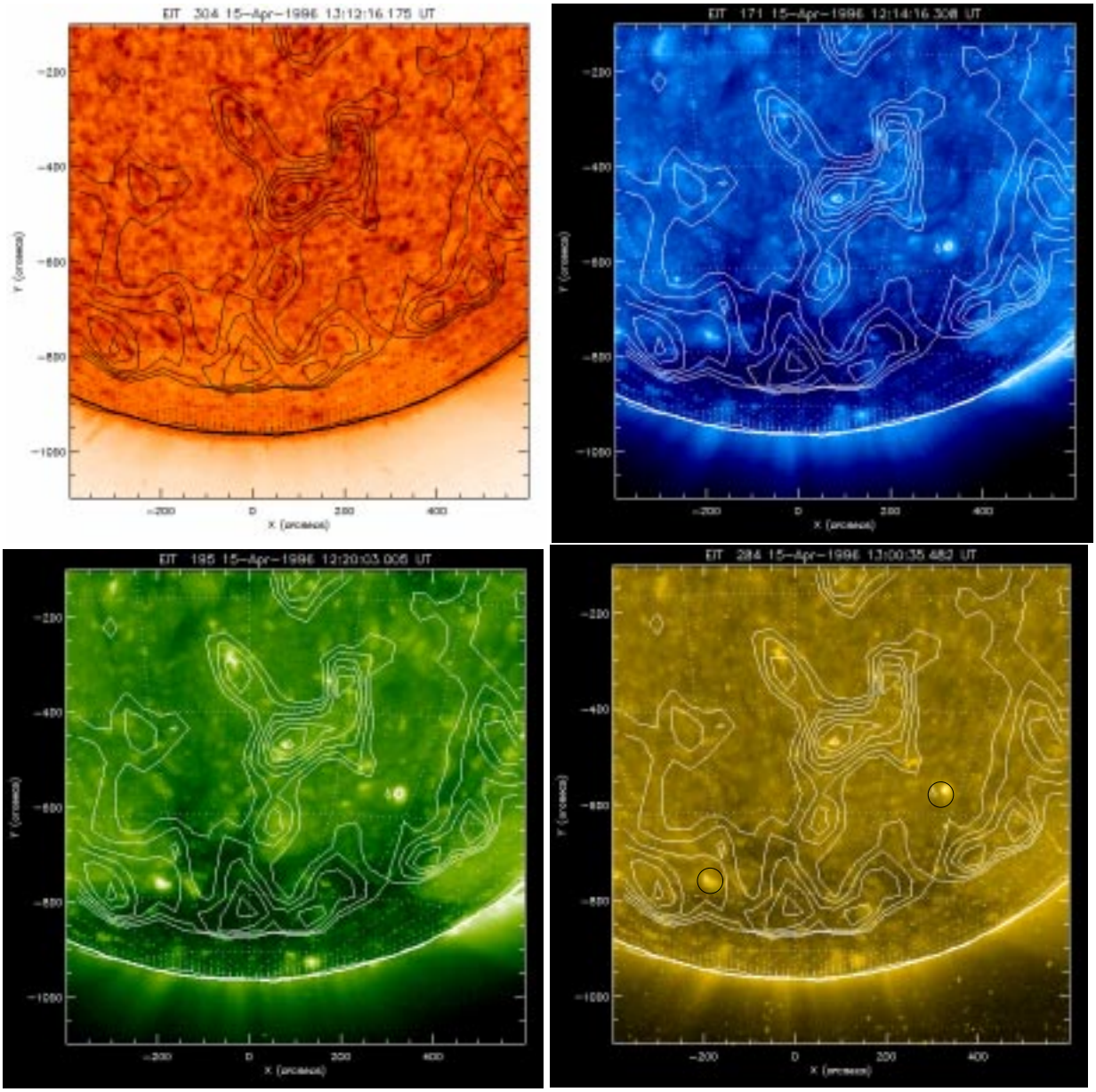

Fig. 29. SOHO/EIT images from the south pole region of the Sun on April 15, 1996: He II (304 Å, $T = 80000$ K, reversed colours) at 13:12 UT (top left), Fe IX/X (171 Å, $T = 1.3$ MK) at 12:14 UT (top right), Fe XII (195 Å, $T = 1.6$ MK) at 12:20 UT (bottom left), and Fe XV (284 Å, $T = 2.0$ MK) at 13:00 UT (bottom right). Superimposed are some selected radio contour lines (white), that show emission above the quiet Sun level (7200 K) at 3.5 mm wavelength at 12:05 − 12:13 UT. The black circles in the Fe XV image (bottom right) show the positions of the EUV and X-ray bright points mentioned in the text. The circles also represent the radio resolution, i.e., a beam size of 60 arcsec. Radio enhancements are seen over the coronal hole and diffuse emission regions, while the EUV bright points only have very faint radio signatures. The same regions are presented in soft X-rays in Fig. 30

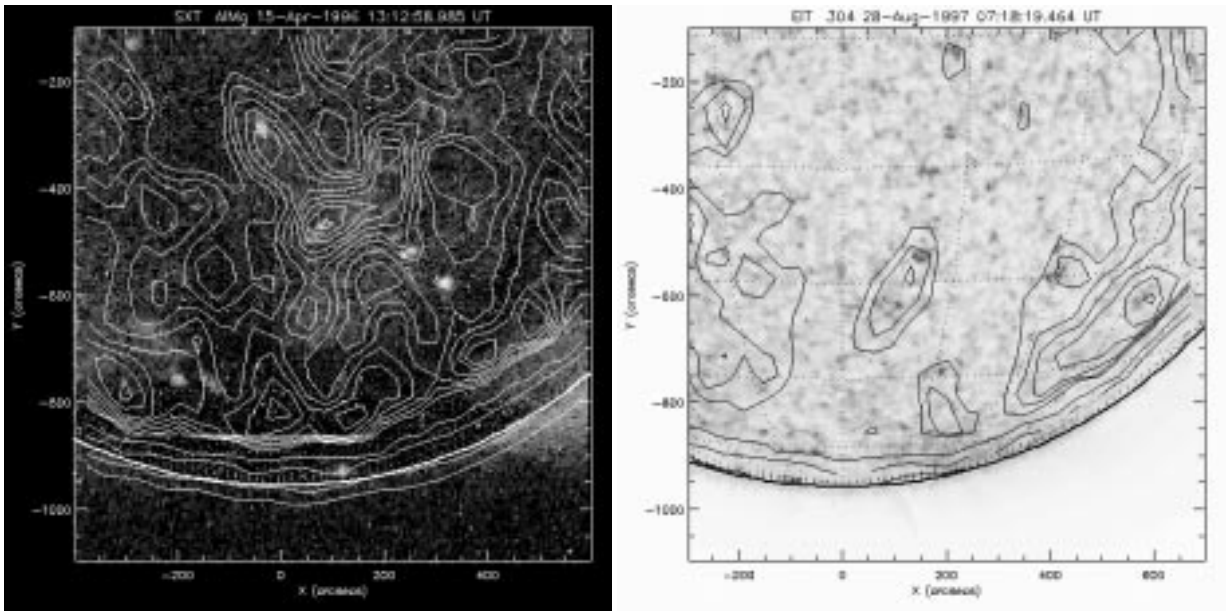

Fig. 30. Left: Yohkoh SXT AlMg image from April 15, 1996, at 13:12:58 UT. The southern coronal hole area is seen in black, and soft X-ray bright points bright. Superimposed are the 3.5 mm radio contours that are above the quiet Sun level, at 12:05 − 12:13 UT. Radio enhancements are seen over the coronal hole area, while the two X-ray bright points (seen in EUV in Fig. 29) only have very faint radio signatures. The emission areas of the two bright points are much smaller in X-rays than in EUV. **Right:** SOHO/EIT He II image on August 28, 1997 at 07:18:19 UT, with the radio map from 07:16 − 07:24 UT superimposed

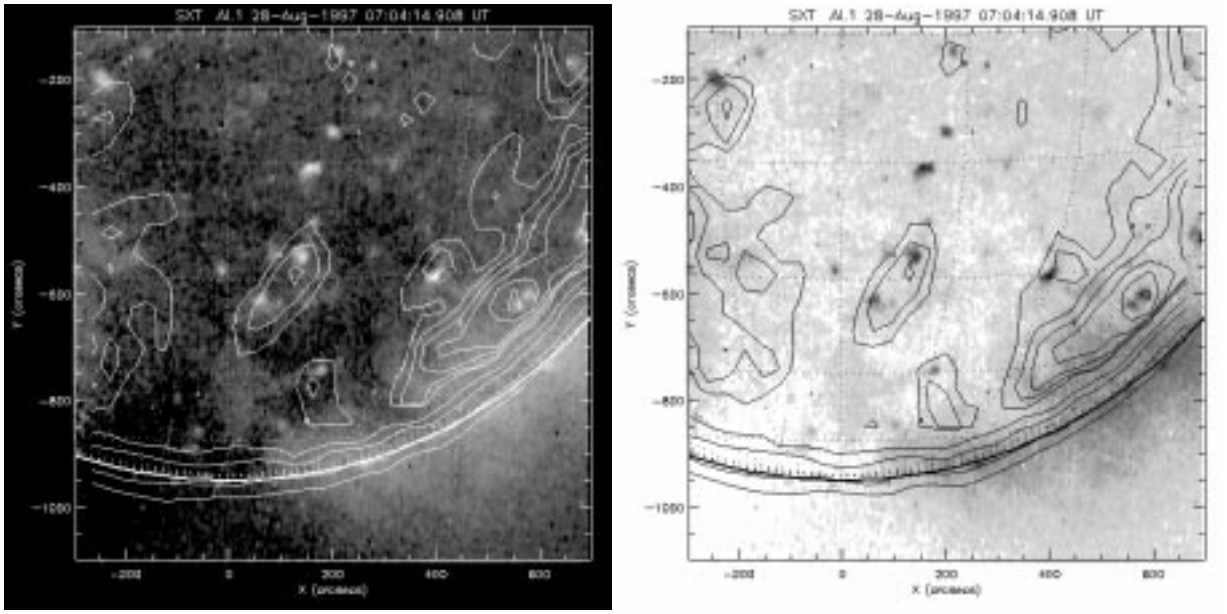

Fig. 31. Left: Radio map observed on August 28, 1997 at 06:56 − 07:05 UT superimposed on the Yohkoh SXT Al.1 image at 07:04:14 UT. **Right**: Radio map observed at 07:16 − 07:24 UT, superimposed on the same Yohkoh SXT map with reversed colors. Radio enhancements are seen in both of the radio maps, at approximately the same locations, that were scanned 19 minutes apart. The enhancements lie over or nearby some X-ray bright points, but the bright point in S16W13 shows no radio emission above the quiet Sun level. Grid spacing in the figure is 15 degrees